Title:

Proximity labeling of Snx14 reveals a functional interaction with Δ-9 desaturase SCD1 to maintain ER homeostasis

Author Line:

Sanchari Datta[1], Jade Bowerman[1], Hanaa Hariri[1], Rupali Ugrankar[1], Kaitlyn M. Eckert[2], Chase Corley[2], Gonçalo Vale[2], Jeffrey G. McDonald[2], Mike Henne[1,*]

Author Affiliation:

[1]Department of Cell Biology, UT Southwestern Medical Center, 6000 Harry Hines Blvd, Dallas, TX 75390; [2]Department of Molecular Genetics, UT Southwestern Medical Center, 6000 Harry Hines Blvd, Dallas, TX 75390

Corresponding author:

Correspondence should be addressed to: mike.henne@utsouthwestern.edu

Key words:

Endoplasmic reticulum (ER); fatty acid (FA); lipid droplet (LD); sorting nexin (SNX); autosomal recessive spinocebellar ataxia 20 (SCAR20)

Abstract:

Fatty acids (FAs) are central cellular metabolites that contribute to lipid synthesis, and can be stored or harvested for metabolic energy. Dysregulation in FA processing and storage causes toxic FA accumulation or altered membrane compositions and contributes to metabolic and neurological disorders. Saturated lipids are particularly detrimental to cells, but how lipid saturation levels are maintained remains poorly understood. Here, we identify the cerebellar ataxia SCAR20-associated protein Snx14, an endoplasmic reticulum (ER)-lipid droplet (LD) tethering protein, as a novel factor required to maintain the lipid saturation balance of cellular membranes. We show that Snx14-deficient cells and SCAR20 disease patient-derived cells are hypersensitive to saturated FA (SFA)-mediated lipotoxic cell death that compromises ER integrity. Using APEX2-based proximity labeling, we reveal the protein composition of Snx14-associated ER-LD contacts and define a functional interaction between Snx14 and Δ-9 FA desaturase SCD1. We show that SCD1 is upregulated in *SNX14*^{KO} cells, and *SNX14*^{KO}-associated SFA hypersensitivity can be rescued by ectopic SCD1 overexpression. The hydrophobic PXA domain of Snx14 and its interaction with SCD1 are required for Snx14-mediated SFA protection function. Lipidomic profiling reveals that *SNX14*^{KO} cells exhibit increased membrane saturation, and mimics the lipid profile of SCD1-inhibited cells. Altogether these mechanistic insights reveal a functional interaction between Snx14 and SCD1 in the ER network to maintain FA homeostasis and membrane saturation, defects in which may underlie the neuropathology of SCAR20.

Significance Statement:

SCAR20 disease is an autosomal recessive spinocerebellar ataxia primarily affecting children, and results from loss-of-function mutations in the *SNX14* gene. Snx14 is an endoplasmic reticulum (ER)-localized protein that localizes to ER-lipid droplet (LD) contacts and promotes LD biogenesis, but why Snx14 loss causes SCAR20 is unclear. Here, we demonstrate that Snx14-deficient cells and SCAR20 patient-derived fibroblasts have defective ER homeostasis and altered lipid saturation profiles. We reveal a functional interaction between Snx14 and fatty acid desaturase SCD1. Lipidomics shows Snx14-deficient cells contain elevated saturated lipids, closely mirroring SCD1-defective cells. Furthermore, Snx14 and SCD1 interact in the ER, and SCD1 over-expression rescues Snx14 loss. We propose that Snx14 maintains cellular lipid homeostasis, the loss of which underlies the cellular basis for SCAR20 disease.

Introduction

Cells regularly internalize exogenous fatty acids (FAs), and must remodel their metabolic pathways to process and properly store FA loads. As a central cellular currency that can be stored, incorporated into membrane lipids, or harvested for energy, cells must balance FA uptake, oxidation, and processing to maintain homeostasis. Defects in any of these processes can elevate intracellular free fatty acids which can act as detergents to damage organelles, or be aberrantly incorporated into membranes. Excessive membrane lipid saturation can alter organelle function and contribute to cellular pathology, known as lipotoxicity [1, 2]. Indeed, failure to properly maintain lipid compositions and lipid storage contributes to many metabolic disorders [3] including type 2 diabetes [4], obesity [5], cardiac failure [6, 7] and various neurological diseases [8].

Properties of FAs such as their degree of saturation and chain length are key determinants of their fate within the cell [9]. High concentrations of saturated FAs (SFAs) in particular are highly toxic to cells, as their incorporation into organelle bilayers affects membrane fluidity and triggers lipotoxicity and cell death [10-13]. To prevent this, cells desaturate SFAs into mono-unsaturated FAs (MUFAs) before they are subsequently incorporated into membrane glycerophospholipids or stored as triglycerides (TG) in lipid droplets (LDs). Indeed, the production of LDs provides a lipid reservoir to sequester otherwise toxic FAs and hence serves as a metabolic buffer to maintain lipid homeostasis [14, 15].

As LDs are created by and emerge from the ER network, inter-organelle communication between the ER and LDs is vital for proper LD biogenesis [16]. Consequently numerous proteins that contribute to LD biogenesis, such as seipin [17, 18] and the diacylglyceride acyltransferase (DGAT) [19], are implicated in ER-LD crosstalk. Previously, we identified Snx14, a sorting nexin (SNX) protein linked to the cerebellar ataxia disease SCAR20 [20-22], as a novel factor that promotes FA-stimulated LD growth at ER-LD contacts [23, 24]. Snx14 is an ER-anchored integral membrane protein. Following addition of the FA oleate, Snx14 is recruited to ER-LD contact sites where it promotes the incorporation of oleate into TG as LDs grow [23]. In line with this, *SNX14*^{KO} cells exhibit defective LD morphology following oleate addition, implying Snx14 is required for proper FA storage in LDs. Related studies of Snx14 homologs in yeast and *Drosophila* indicate a conserved role for Snx14 family proteins in FA homeostasis and LD biogenesis [25, 26].

Despite these insights, why humans with Snx14 loss-of-function mutations develop the cerebellar ataxia disease SCAR20 remains enigmatic. Given the proposed role of Snx14 in FA metabolism, and that numerous neurological pathologies arise through defects in ER lipid homeostasis [27-29], here we investigated whether Snx14 loss alters the ability of cells to maintain lipid homeostasis. Our findings indicate that Snx14-deficient cells are hypersensitive to SFA exposure, and manifest

defects in ER morphology and ER-associated lipid metabolism. In line with this, APEX2-based proteomics identifies Snx14-associated factors at ER-LD contacts that maintain lipid homeostasis. In particular, here we identify a functional interaction between Snx14 and the Δ-9 FA desaturase SCD1, which converts SFAs into MUFAs in the ER network. Consistent with this, *SNX14*^{KO} cells depend on SCD1 function to maintain lipid and cellular homeostasis. Lipidomic profiling reveals altered SFA incorporation into glycerophospholipids and neutral lipids in *Snx14*^{KO} cells which mimic lipid alterations in SCD1-inhibited cells, indicating that Snx14 loss mirrors SCD1 functional inhibition. These observations provide important new insights into the cellular basis of Snx14 function, the loss of which contributes to SCAR20 disease.

Results:

SNX14^{KO} cells are hypersensitive to saturated fatty acid associated lipotoxicity

Previously, we showed that following oleate addition, Snx14 enriches at ER-LD contacts to promote LD growth, and Snx14 loss disrupts LD homeostasis [23]. To further dissect Snx14 function in maintaining lipid homeostasis, we interrogated how *SNX14*^{KO} cells responded to different saturated and unsaturated FA species. We exposed wildtype (WT) or *SNX14*^{KO} *U2OS* cells to titrations of specific SFAs or MUFAs for 48 hours, and monitored cell viability following FA exposure using an established crystal violet assay [30, 31]. Exposure to MUFAs including palmitoleate (16:1) and oleate (18:1) did not perturb cell viability of either WT or *SNX14*^{KO} cells even at 1000μM concentrations (**Fig 1 A, A'**). In contrast, treatment of WT cells with increasing concentrations of SFAs such as palmitate (16:0) or stearate (18:0) resulted in decreased cell survival, as previously reported [13, 32] (**Fig 1 B, B'**).

Intriguingly, *SNX14*^{KO} *U2OS* cells were hyper-sensitive to SFA-induced death compared to WT cells (**Fig 1 B, B'**). The concentration of palmitate at which ~50% of WT cells survive is ~1000μM, but only ~500μM for *SNX14*^{KO} (**Fig 1B**). Similarly, exposure to ~600μM stereate resulted in ~50% cell viability for WT cells, but only required ~300μM for *SNX14*^{KO} (**Fig 1B'**). Consistent with this, SCAR20 patient-derived fibroblasts [20, 24] which lack Snx14 (*SNX14*^{Mut}) exhibited significantly reduced cell viability compared to control fibroblasts following palmitate addition (**Fig 1C**). *SNX14*^{Mut} cells reached ~50% viability at ~1000μM palmitate exposure whereas more than 50% WT cells were viable even at 2000μM palmitate treatment. Collectively, these observations indicate that Snx14-deficient cells are hyper-sensitive to SFA exposure.

Once internalized, free FAs are esterified with CoA and can be shunted into several distinct metabolic fates, including their incorporation into ceramides [33], glycerophospholipids [34], or neutral lipids[35]. They can also be harvested by catabolic breakdown in oxidative organelles such as mitochondria [2]. To begin to dissect why *SNX14*^{KO} cells were hyper-sensitive to SFAs, we conducted a systemic

analysis of each of these FA-associated pathways. Since intracellular ceramide accumulation can itself be toxic [33], we first tested whether pharmacologically lowering ceramide synthesis could rescue the SFA-associated toxicity in *SNX14*^{KO} cells. We treated cells with myriocin, which inhibits the SPT complex that incorporates palmitate into newly synthesized ceramides [10]. Myriocin treatment did not rescue *SNX14*^{KO} SFA hypersensitivity, suggesting that elevated ceramides does not contribute to *SNX14*^{KO} palmitate-induced cell death (**Fig 1D**). Next, we examined whether mitochondrial FA oxidation was required for *SNX14*^{KO} hypersensitivity [36, 37]. We pharmacologically inhibited mitochondrial FA uptake via etomoxir treatment, but this did not suppress palmitate-induced lipotoxicity in *SNX14*^{KO} cells (**Fig 1E**). This indicates that *SNX14*^{KO} cells are not sensitive to palmitate due to alterations in mitochondrial FA oxidation.

SFA-induced toxicity in *SNX14*^{KO} cells is associated with defects in ER morphology

A major FA destination is their incorporation into membrane glycerophospholipids via *de novo* lipid synthesis at the ER. As such, a major contributor of lipotoxic cell death is the incorporation of excessive SFAs into diacyl-glycerophospholipids, which impacts ER membrane fluidity and causes cellular stress [12, 38]. To determine whether excessive SFA exposure affected ER homeostasis in *SNX14*^{KO} cells, we examined ER morphology of WT and *SNX14*^{KO} cells exposed to palmitate via fluorescence confocal microscopy. Whereas the immunofluorescently stained ER network of WT cells was reticulated and regular following 16hrs exposure to 500μM palmitate, *SNX14*^{KO} cells displayed perturbed ER morphology. The ER of *SNX14*^{KO} cells appeared fragmented, and contained drastic bulges within the tubular network following palmitate treatment (**Fig 2A; red arrows**). These features became more prominent when we examined the ER ultrastructure with high-resolution transmission electron microscopy (TEM). Here, WT and *SNX14*^{KO} cells were either left untreated or cultured in media containing 500μM of palmitate for 6hrs or 16hrs, fixed, and processed for thin-section TEM. WT cells exhibited normal tubular ER networks and did not manifest any significant change in the ER morphology when exposed to palmitate (**Fig. 2B**). Similarly, *SNX14*^{KO} cells not exposed to palmitate exhibited normal ER morphology. In contrast, the ER of *SNX14*^{KO} cells exposed to 6hrs palmitate appeared swollen and dilated, forming sheet-like extensions within the thin-section plain (**Fig 2B; red arrows**). The ER dilation of *SNX14*^{KO} cells was more pronounced following 16hrs treatment (**Fig 2B; red arrows**). Collectively, these observations suggest that *SNX14*^{KO} cells manifest altered ER architecture following prolonged exposure to palmitate.

APEX-based proteomics reveals Snx14 interacts with proteins involved in SFA metabolism at ER-LD contacts

Given that Snx14 was required for maintaining ER morphology following prolonged palmitate exposure, we next investigated what proteins Snx14 interacted with that may promote ER homeostasis. Previously we utilized proximity-based technology based on the ascorbate peroxidase APEX2 to examine the localization of APEX2-tagged Snx14 at ER-LD contact sites using TEM [23]. APEX2-tagging also enables the local interactome of a protein-of-interest to be interrogated. The addition of biotin-phenol and hydrogen peroxide to APEX2-expressing cells induces the local biotinylation of proteins within ~20nm of the APEX2 tag. These biotinylated proteins can be subsequently affinity purified via streptavidin beads and identified via mass-spectrometry (MS) [39] (**Fig 3A**). As ER-LD contacts are lipogenic ER sub-domains with known roles in FA processing, we hypothesized that Snx14's enrichment at ER-LD junctions represented an opportunity to identify proteins in close proximity to Snx14 that contribute to lipid processing. We thus used APEX2-based proteomic screening to interrogate the protein composition of Snx14-associated ER-LD contacts under these conditions.

We generated *U2OS* cells stably expressing Snx14-EGFP-APEX2 and *HEK293* cells transiently expressing Snx14-EGFP-APEX2 and exposed them to oleate to induce Snx14 recruitment to ER-LD contacts, then treated them with biotin-phenol for 30 minutes and hydrogen peroxide for 1 minute. As expected, co-immunofluorescence staining of *U2OS* cells for Streptavidin-Alexa647 and EGFP revealed their colocalization, suggesting that proteins in close proximity to Snx14-EGFP-APEX2 at ER-LD contacts became biotinylated (**Fig 3B**). This was further confirmed when both *U2OS* and *HEK293* labeled cell lines were lysed and the biotin-conjugated proteins affinity purified with streptavidin beads. Gel electrophoresis and anti-streptavidin/HRP Western blotting of streptavidin affinity-purified lysates revealed many biotinylated proteins in Snx14-EGFP-APEX2-expressing cell lysates, but not in the control lacking APEX2 (**Fig 3C**). The bead enriched biotinylated proteins from both Snx14-EGFP-APEX2 and the control lacking APEX2 were then identified by tandem MS/MS proteomic analysis.

To identify potential Snx14 interactors, we implemented a multi-stage analysis approach (**Fig 3D**). First, we selected proteins that were greater than 2.0-fold enriched in Snx14-EGFP-APEX2 samples over the negative controls lacking APEX2 for both *U2OS* and *HEK293* cell lines. Next, we focused on proteins known to localize to the ER network, since this was the primary organelle that Snx14 localized to, and the organelle that manifested morphological alterations in *SNX14*^{KO} cells following palmitate exposure. We did this analysis in two stages. First, we eliminated proteins that may non-specifically interact with an APEX2 tag simply localized at the ER surface. We generated cell lines expressing cytoplasmic-facing APEX2 tagged to Sec61β, and conducted APEX2 proximity labeling and MS-based proteomics in these cells (**Fig S3 A**). By comparing the Snx14-EGFP-APEX2 and APEX2-Sec61β protein lists, we excluded proteins that were also enriched 2.0-fold or more in APEX2-Sec61β compared to negative control in either the *U2OS* and *HEK293* cell lines (>1.0 of $\log_2$(value) in the 1st, 2nd and 4th quadrants of **Fig S3 A**). This

generated a new list of 2376 candidate proteins only enriched in the Snx14-EGFP-APEX2 proteomics (**Supplementary Table 1; Fig 3 E, and 3rd quadrant of Fig S3 A**). As expected, in addition to many ER proteins, many LD-associated proteins including PLIN2, PLIN3, LPCAT1, and ACSL4 were also detected in this Snx14 interactome (several noted in **Fig S3 B**). We also detected the diacylglycerol o-acyltransferase DGAT1, which we previously determined was influenced by Snx14 *in vitro* during FA-stimulated TG synthesis [23] (**Fig 3E**). Of note, PLIN3 was enriched ~65-fold in both cell line samples, similar to Snx14 enrichment (**Fig 3E**). This might be because PLIN3 is a perilipin protein that associates with newly formed LDs, and Snx14 enriches at ER-LD during oleate stimulated LD biogenesis. As a second stage of focusing on ER-localized proteins, we applied gene ontology enrichment analysis on these 2376 candidate proteins to identify 305 of them known to localize to the ER (**Fig 3F**). Notably, ~250 of these ER-resident genes are associated with cellular metabolism, and ~100 of them are involved in lipid metabolism (**Fig S3 D**).

With this smaller candidate list, we next compared our proteomics to a recently published genome-wide CRISPR/Cas9 screen that identified genes whose deletion sensitized cells to palmitate-induced lipotoxicity [40]. Consistent with our observations, this unbiased screening identified Snx14 in the top 6% of genes that were protective against palmitate (KO gene score: -2.28). Indeed, this study identified 310 proteins which exhibited a negative gene score greater than -1.8 [40], and were also enriched in our Snx14 interactome (**Supplementary Table 2; orange dots of Fig 3E; Fig S3 C**). Intriguingly, this list contained many proteins involved in lipid desaturation including FADS1, FADS2, SCD1, CEPT1 and HSD17B12 (**Fig S3 B**).

As a final stage of analysis, we compared our list of Snx14 interactors to the recently published interactome of Snx14 *Drosophila melanogaster* ortholog Snz, which also functions in LD homeostasis in fruit fly adipocytes [26]. Snz proteomics identified the enzyme DESAT1, the major Δ-9 FA desaturase, as a key Snz interactor that is required for Snz-driven TG synthesis in *Drosophila* [26]. DESAT1 is the ortholog of human Δ-9 FA desaturase SCD1, which catalyzes the conversion of SFAs to MUFAs prior to their incorporation into glycerophospholipids or neutral lipids [41]. Indeed, SCD1 was enriched ~7 fold in Snx14-EGFP-APEX2 proteomics in both *U2OS* and HEK293 cell lines (**Fig 3E**). Notably, SCD1 genetic or pharmacological perturbation hyper-sensitizes cells to SFA-induced lipotoxicity [13, 42, 43] (**Fig S5 A**). SCD1 was also identified in genome-wide CRISPR/Cas9 screening for palmitate hyper-sensitivity, and scored similarly as Snx14 (SCD1: -2.42, Snx14: -2.28) [40]. Based on this analysis, we chose to investigate whether Snx14 and SCD1 functionally interact.

ER association of Snx14 is necessary for its interaction with SCD1

To begin to investigate whether Snx14 and SCD1 functionally interact, we first determined whether they co-immunoprecipitate (co-IP). We generated *U2OS* cell lines stably expressing either 3xFlag-tagged Snx14 or 3xFlag-tagged GFP,

conducted anti-Flag immuno-precipitation, and Western blotted the IP lysates for endogenous SCD1. An interaction of Snx14 and SCD1 was detected as Snx14-Flag could co-IP endogenous SCD1, but GFP-Flag could not (**Fig 4A**). Intriguingly, Snx14-Flag could co-IP SCD1 both with and without the addition of exogenous palmitate (**Fig 4A**). To confirm that this co-IP detected a specific interaction between Snx14 with SCD1, we interrogated whether we could detect other proteins found in high abundance in the Snx14-EGFP-APEX2 proteomics. We Western blotted for PLIN3 which was highly enriched (>60-fold) in the Snx14 APEX2-proteomics (**Fig 3E**). Notably, PLIN3 was not detected in the Snx14 co-IP lysate, indicating the interaction with SCD1 was specific (**Fig S4A**). Next we dissected what regions of Snx14 were sufficient to co-IP SCD1. We used previously generated cell lines stably expressing the N-terminal half of Snx14 containing the transmembrane (TM), PXA, and RGS domains ($Snx14^{N}$), or a C-terminal half expressing only the PX and C-Nexin domains ($Snx14^{PXCN}$) (**Fig 4B**). This revealed that $Snx14^{N}$, but not $Snx14^{PXCN}$, was sufficient to interact with SCD1, albeit this interaction was reduced compared to full length Snx14 (**Fig 4C**). To test whether the Snx14:SCD1 interaction required SCD1 desaturase activity, we conducted a co-IP of SCD1 with full length Snx14 ($Snx14^{Fl}$) in the presence of a commercially available SCD1 inhibitor (SCD1i) [44]. Surprisingly, inhibited SCD1 still co-IPed with $Snx14^{Fl}$, indicating their interaction did not require SCD1 enzymatic activity (**Fig 4C**).

Next we determined whether Snx14 and SCD1 co-localize *in vivo* by conducting immunofluorescence (IF) confocal imaging of endogenous SCD1 in *U2OS* cells stably expressing EGFP-tagged Snx14 fragments. IF labeling of SCD1 in WT cells revealed its localization throughout the ER network following OA treatment. However, in cells expressing full length Snx14-EGFP, SCD1 accumulated at Snx14-EGFP-positive punctae adjacent to LDs following oleate treatment, suggesting SCD1 was recruited to ER-LD contacts together with Snx14-EGFP (**Fig 4D red arrows, S4 B**). In contrast, expression of $Snx14^{PXCN}$-EGFP, which can also localize to ER-LD contacts, failed to recruit SCD1, consistent with the N-terminal fragment of Snx14 being required for the SCD1 interaction (**Fig 4D, S4 B**). As expected, $Snx14^{N}$-EGFP localized throughout the ER network following OA treatment as previously observed, since it lacks the LD-targeting CN domain, but this co-localized with endogenous SCD1 throughout the ER network and did not induce SCD1 accumulation surrounding LDs (**Fig 4D, S4B**). Collectively, this suggests that Snx14 interacts with SCD1 via its N-terminal region and is sufficient to co-IP SCD1 from cell lysates as well as recruit SCD1 to ER-LD contacts *in vivo*.

SCD1 activity can rescue *SNX14*^{KO} palmitate-induced lipotoxicity

Next we investigated how the Snx14:SCD1 interaction influences lipid homeostasis following palmitate treatment. Through Western blotting we noted that SCD1 protein levels were elevated in *SNX14*^{KO} cells compared to WT following treatment with 500μM of palmitate, implying *SNX14* deletion elevated SCD1 protein levels,

potentially as a cellular compensatory mechanism (**Fig 5A, B**). Snx14-Flag over-expressing cells returned SCD1 protein levels to WT levels, suggesting that Snx14 loss was causative for the elevated SCD1 protein level. In line with this, pharmacological inhibition of SCD1 further hyper-sensitized *SNX14*^{KO} cells to palmitate treatment, indicating that *SNX14*^{KO} cells were highly reliant on SCD1 activity in the presence of palmitate to maintain viability (**Fig S5 A**). This also indicated that, although SCD1 protein levels are increased with Snx14 loss, this increase is not sufficient to reduce *Snx14*^{KO} associated SFA hypersensitivity.

To dissect this further, we queried whether ectopic over-expression of SCD1 could reduce palmitate hyper-sensitivity observed in *SNX14*^{KO} cells. Strikingly, SCD1 over-expression rescued *SNX14*^{KO} cell viability following palmitate exposure, and *SNX14*^{KO} cells now responded similarly to WT cells exposed to dose-dependent palmitate treatment (**Fig 5C**). *SNX14*^{KO} cells were also rescued by exposure to a 10:1 mixture of palmitate and oleate, the MUFA and product of SCD1 enzymatic activity (**Fig 5D**). Since LDs are lipid reserviors, we determined whether this SCD1-mediated rescue required the incorporation of FAs into TG for LD storage. We exposed *SNX14*^{KO} cells to DGAT1/2 inhibitors (DGATi) in the presence of palmitate, and monitored cell viability. Surprisingly, SCD1 over-expression rescued *SNX14*^{KO} cells similarly even in the presence of DGATi, suggesting SCD1 rescue functions upstream of TG synthesis (**Fig 5E**). Collectively, these observations imply that *SNX14*^{KO} cells exhibit defects in FA metabolism upstream of TG synthesis which can be rescued by SCD1 over-expression or the exogenous addition of MUFAs.

To further understand whether the Snx14:SCD1 interaction is necessary and sufficient to rescue palmitate hyper-sensitivity of *SNX14*^{KO}, we dissected what regions of Snx14 were necessary and sufficient to rescue *SNX14*^{KO} cell viability. We stably re-introduced several Flag-tagged Snx14 constructs into *SNX14*^{KO} cells and monitored cell viability following 500μM palmitate treatment. As expected, Snx14^{FL} but not the empty vector (EV) were able to rescue viability back to WT levels (**Fig 5F**). Intriguingly, introduction of Snx14^{N} could rescue *SNX14*^{KO} cells (**Fig 5F**), suggesting that the N-terminal half of Snx14, which was sufficient to interact with SCD1 (**Fig 4C**), was also sufficient to rescue Snx14 loss. In contrast, Snx14^{PXCN} did not rescue *SNX14*^{KO} sensitivity, consistent with its inability to co-IP with SCD1 (**Fig 5F, 4C**). Further dissection revealed that a Snx14 construct which lacked the N-terminal TM domain but encoded all other domains (Snx14$^{FL\Delta TM}$) could not rescue the *SNX14*^{KO} cell viability, indicating that ER association by the TM region was required for Snx14 function (**Fig 5G,F**). Notably, expression of a full length version of Snx14 that lacked the N-terminal hydrophobic PXA domain (Snx14$^{FL\Delta PXA}$) failed to rescue *SNX14*^{KO} cell palmitate sensitivity, indicating that the PXA domain is necessary for Snx14 function (**Fig 5F**).

Finally, to understand whether the failure of Snx14$^{FL\Delta TM}$ and Snx14$^{FL\Delta PXA}$ to rescue *SNX14*^{KO} hyper-sensitivity was linked to their inability to interact with SCD1, we

determined whether Snx14$^{FL\Delta TM}$ and Snx14$^{FL\Delta PXA}$ could co-IP SCD1. Whereas Snx14$^{FL\Delta TM}$ failed to co-IP SCD1, Snx14$^{FL\Delta PXA}$ was able to co-IP SCD1 (**Fig 5G, H**). Collectively, these experiments indicate several conclusions: 1) the Snx14 TM region is necessary for both SCD1 interaction and Snx14 function following palmitate exposure. 2) The PXA domain, which related studies using the Snx14 yeast ortholog Mdm1 has been shown to directly bind to FAs *in vitro* [25], is also essential for Snx14 function, although it is not required for the Snx14:SCD1 co-IP interaction. 3) Finally, the Snx14^{N} construct, which contains only the TM, PXA, and RGS domains, is sufficient to rescue *SNX14*^{KO} palmitate hyper-sensitivity.

SNX14^{KO} cells display an altered lipidomic profile

Following its absorption, palmitate is esterified, and much of it becomes mono-unsaturated prior to its incorporation into other lipid species [45]. Since SCD1 desaturates esterified SFAs such as palmitate, and Snx14 functionally interacts with SCD1, we next directly examined the ability of *SNX14*^{KO} cells to process palmitate. We exposed WT and *SNX14*^{KO} cells to 500µM palmitate for 0, 2, 4, 8, and 16 hr, extracted whole cell lipids and conducted thin layer chromatography (TLC) to monitor changes in free FAs (FFAs) and neutral lipids. As expected both WT and *SNX14*^{KO} cells exhibited elevated FFA levels following 2 and 4 hrs palmitate exposure, but *SNX14*^{KO} exhibited signiatantly elevated FFAs (**Fig 6 A, A'**). Remarkably, SCD1 over-expression reversed the FFA elevation at 4 hrs in *SNX14*^{KO} cells, implying the elevated FFA pool was composed of SFAs that could be processed by SCD1 (**Fig 6 B, B'**). Relatedly, SCD1 over-expression also rescued *SNX14*^{KO} ER fragmentation following overnight palmitate exposure (**Fig 6C**). Collectively, this indicates that *SNX14*^{KO} cells accumulate FFAs following palmitate exposure consistent with a defect in palmitate processing, and these effects can be reversed by SCD1 overexpression.

Snx14 loss elevates saturated fatty acyl groups in polar lipids

To understand how ER morphology is altered in palmitate-treated *SNX14*^{KO} cells, we investigated whether Snx14 loss alters membrane lipid synthesis at the ER. We conducted whole-cell lipidomic FA profiling of the polar lipid fraction of WT and *SNX14*^{KO} cells. We pulsed WT and *SNX14*^{KO} cells for 2 hours with 500µM palmitate, extracted polar lipids, and conducted GC-MS analysis to profile for their fatty acyl chain length and saturation types. Indeed, *SNX14*^{KO} cells exhibit a significant increase in total polar lipid-derived FAs (**Fig S6 A**), as well as a significant increase in the abundance of 16-carbon length saturated fatty acyl chains (FA|16:0) in the polar lipids relative to WT cells (**Fig 6D**). To determine whether this increase mimics alterations in polar lipids when SCD1 function is perturbed, we also treated WT cells with SCD1 inhibitor (SCD1i). Strikingly, WT cells exposed to SCD1i exhibited similar increases in 16:0 saturated fatty acyl chains in their polar lipid fraction, mirroring elevations observed in *SNX14*^{KO} cells (**Fig 6D**). Furthermore, *SNX14*^{KO} cells treated

with SCD1i exhibited no additional 16:0 acyl chain increases in the polar lipid profile. This suggests that *SNX14*^{KO} cells contain elevated saturated fatty acyl chain incorporation into polar lipids following palmitate treatment, similar to cells where SCD1 function is inhibited. Additionally, Snx14 loss does not futher alter the FA profile of SCD1 inhibited cells, implying these two perturbations exist on the same pathway of lipid processing.

TG, PC, and lysolipids lipids exhibit significant elevations in saturated acyl chains in *SNX14*^{KO} cells

To further dissect how the abundances and fatty acyl compositions of specific lipid classes are altered by Snx14 loss, we conducted global lipidomics via quantitative LC-MS analysis. WT and *SNX14*^{KO} cells were either left untreated or exposed to 2 hr of palmitate, harvested, and analyzed. For comparative analysis, we also treated cells with SCD1i. Importantly, this LC-MS analysis revealed the fatty acyl properties such as chain length and saturation types of major lipid classes, including TG, diacylglyceride (DAG), phosphatidylethanolamine (PE), phosphophatidylcholine (PC), phosphatadic acid (PA), phosphatidylserine (PS), and lysophospholipids. Analysis revealed a significant (~40%) increase in the levels of DAG, LPE and PC in *SNX14*^{KO} cells relative to WT cells following palmitate treatment as calculated from the fold change percentage of the color-coded heat map (**Fig 7A**). However, relative abundances of most lipid classes between these two species with or without palmitate treatment were not altered.

Next we examined the change in the saturation of the acyl chains within each lipid class in *SNX14*^{KO} cells. In general, there was a greater proportion of saturated fatty acyl chains within many lipid classes. Among different lipid classes, the most significant change in saturated fatty acyl chains in palmitate-treated *SNX14*^{KO} cells relative to WT was in TG and lyso-PC (LPC). In fact, evaluation of the FA profile of ~60 different TG species revealed the most significant increase in TG species containing two or more saturated acyl chains. These TG species contained either 0 or only 1 unsaturation among all three acyl chains (denoted as an N score of 0 or 1) (**Fig 7B**). For example, TG|48:1(NL-16:1), which contains one 16:1 acyl chain and two fully saturated acyl chains, was significantly elevated in *SNX14*^{KO} cells following palmitate treatment (**Fig 7B, species 11**). Similarly, TG 50:0 (NL-16:0) and 50:0 (NL-18:0), both of which contained fully saturated acyl chains, were also elevated in *SNX14*^{KO} cells compared to WT following palmitate addition and SCD1 inhibition, suggesting *SNX14*^{KO} cells incorporated SFAs into TG more than WT cells (**Fig 7B, species 1 and 2**). For more general analysis, we pooled the abundances of all TG species comprising only 0 or 1 total unsaturations within their fatty acyl chains to derive a general overview of how these TG species were altered in *SNX14*^{KO}. As expected, total TG species containing 0 or 1 unsaturation were significantly increased in palmitate treated *SNX14*^{KO} cells, and closely mirrored levels of WT cells treated with SCDi (**Fig 7C**). Collectively, this suggests that the TG lipid profile of

SNX14^{KO} cells treated with palmitate appears similar to cells with inhibited SCD1 function.

Among polar lipid species, the abundance of LPC species containing the saturated fatty acyl chain 18:0 exhibited a significant increase in palmitate treated *SNX14*^{KO} cells relative to WT, and this was further elevated with additional SCDi inhibition (**Fig 7D**). In fact, levels of 18:0-containing LPC in *SNX14*^{KO} cells treated with palmitate mirrored WT cells treated with palmitate and SCD1i, again indicating that *SNX14*^{KO} cells closely resembled cells with inhibited SCD1 function by lipid profiling (**Fig 7D**). Additionally, LPE species containing 18:0 fatty acyl chains were significantly increased in *SNX14*^{KO} cells even without palmitate treatment (**Fig S7A**). Profiling of PC, one of the most abundant glycerophospholipids, revealed an increase in PC species with 18:0 fatty acyl chain in *SNX14*^{KO} cells, and that was more pronounced with palmitate treatment followed by SCD1 inhibition (**Fig S7B**). PS lipid profiles were similarly altered in *SNX14*^{KO}, with increases in PS species containing 18:0 saturated fatty acyl groups (**Fig S7C**). Collectively this suggests that: 1) *SNX14*^{KO} cells exhibit elevated levels of TG species containing two or more saturated acyl chains. 2) *SNX14*^{KO} cells exhibit increased levels of LPC and LPE lysolipids containing saturated fatty acyl chains, and 3) *SNX14*^{KO} cells also exhibit elevated PC and PS phospholipids containing saturated fatty acyl groups. 4) For TG and LPC, the lipid profiles of *SNX14*^{KO} cells exposed to palmitate closely mirror cells with inhibited SCD1 function. Given that Snx14 and SCD1 co-localize within the ER network and co-IP biochemically, this implies that Snx14 loss leads to mis-functional or hypomorphic SCD1 activity that alters the lipid profile of cells.

Discussion:

FAs are essential cellular components that act as energy substrates, biomembrane components, and key signaling molecules. These functions are dependent on the chemical features of FAs such as their chain length and saturation degree, which influence membrane fluidity and impact organelle structure and function [10, 40]. As such, proper FA utilization depends on proper FA processing and channeling to specific organelle destinations. When cells are exposed to high concentrations of exogenous FAs, they respond by elevating FA processing and storage to cope with the excess lipid stress. Excess FAs are incorporated into neutral lipids to be stored in LDs, which protect cells from lipotoxicity [46]. Much of the machinery to achieve this resides at the ER, and proper ER-LD crosstalk by proteins such as seipin and the FATP1-DGAT2 complex is essential to maintain proper lipid homeostasis [17-19]. Our earlier work revealed a role for Snx14 in ER-LD crosstalk, the loss of which contributes to the cerebellar ataxia disease SCAR20 for unknown reasons [23]. Here, we report the proteomic composition of Snx14-associated ER-LD contacts, and provide mechanistic insights into the molecular function of Snx14 that reveal a critical role for Snx14 in lipid metabolism via a functional interaction with FA

desaturase SCD1. We find that Snx14 loss impacts the ability of exogenous SFAs to be mono-unsaturated. In line with this, *SNX14*^{KO} cells display elevated SFA incorporation into membrane glycerophospholipids, lyso-phospholipids, and TG, which impacts ER morphology and ultimately cell homeostasis.

Through systematic interaction analysis and biochemistry, we identify a functional interaction between Snx14 and the Δ-9-FA desaturase SCD1 (**Fig 8**), which catalyzes the oxidization of SFAs to MUFAs [41]. SCD1 enzymatic inhibition alters membrane lipid composition by increasing the incorporation of saturated fatty acyl chains into membrane lipids, which ultimately affects membrane fluidity and organelle function [12, 47]. Consequently, SCD1 protein levels are tightly controlled by cells, as low levels of SCD1 are protective against obesity and insulin resistance whereas complete SCD1 loss promotes inflammation and stress in adipocytes, macrophages, and endothelial cells [47-49].

Initially we observed that *SNX14*^{KO} cells were hyper-sensitive to SFA exposure, similar to SCD1 inhibitory effects, and exhibited defects in ER morphology. Consistent with this, a separate study reporting global CRISPR-based screening identified Snx14 loss as hyper-sensitizing to palmitate exposure [40]. Our subsequent investigation here indicates a functional interaction between Snx14 and SCD1 in protecting cells from SFA-associated lipid stress, based on several observations. First, we find that SCD1 is enriched in the interactome of APEX2-tagged Snx14 via mass spectrometry-based proteomics from two different tissue culture cell lines. Whereas this APEX2 labeling was used previously to analyze the proteomic composition of LDs [50], here we have capitalized on the ability of Snx14 to localize to ER-LD contacts to interrogate the local interactome of this inter-organelle junction. This revealed that SCD1 as well as other proteins involved in LD biogenesis (DGAT1 and PLIN3) are enriched at ER-LD contacts. Among these proteins, we detect a functional interaction between Snx14 and SCD1, and this interaction occurs via Snx14's ER-anchored region. Indeed, ectopic Snx14-EGFP expression can re-localize endogenous SCD1 from throughout the ER network to ER-LD contact sites upon exogenous FA addition, indicating that the Snx14:SCD1 protein-protein interaction occurs within cells. Second, we observe that *SNX14*^{KO} cells exhibit naturally elevated SCD1 protein levels, implying metabolic rebalancing in the absence of Snx14 that requires additional SCD1 activity. However, this elevated SCD1 protein level appears insufficient to rescue *SNX14*^{KO} cell SFA hyper-sensitivity, which can be rescued with a further increase in SCD1 protein levels by ectopic SCD1 overexpression. Finally, through quantitative lipidomic analysis, we observe that *SNX14*^{KO} cells exhibit elevated SFA levels following pulse-experiments with palmitate. KO cells also show increased incorporation of saturated acyl-chains into TG and several phospholipid and lyso-phospholipid species. We also demonstrate that this altered *SNX14*^{KO} lipid profile closely mimics cells with SCD1 pharmacological inhibition, underscoring that Snx14 loss is functionally similar to perturbed SCD1 function (**Fig 8**).

Collectively, our observations indicate a functional interaction between Snx14 and SCD1, and that Snx14-deficient cells have perturbed SCD1 function. Although we do not understand the exact molecular nature of the Snx14:SCD1 interaction, or why Snx14 loss impacts SCD1 function, there are several possibilities. Snx14 may stimulate SCD1 enzymatic activity by allosterically interacting with SCD1 within the ER network. Alternatively, Snx14 may supply FA substrates to SCD1 to convert into MUFAs. Consistent with this, *in vitro* studies on Snx14 yeast ortholog Mdm1 indicate that the PXA domain binds to FAs [25]. In line with this, our present work indicates that the Snx14 PXA domain is required for protection against SFA-mediated lipotoxicity (**Fig 5F**). A third possibility is that Snx14 acts as a scaffold within the ER to recruit SCD1 into ER sub-domains where FA desaturation locally occurs. Given that Snx14 localizes to ER-LD contact sites, which are lipogenic sub-domains known to contain DGAT enzymes for instance, this model is attractive, and positions Snx14 to function as a “metabolic scaffold” that attracts or organizes FA metabolism proteins into regions of the ER in close proximity to LDs, where newly generated MUFAs are easily incorporated into TG or phospholipids. Consistent with this, we also detect FA elongase ELOVL1 and other FA desaturases such as FADS1 and FADS2 in our Snx14 APEX2 interactome, indicating that Snx14-positive ER-LD contacts contain several enzymes involved in multiple stages of FA processing such as elongation and polyunsaturated FA (PUFA) synthesis, respectively. Furthermore, other scaffolding proteins at ER-LD contacts such as seipin require PUFAs to be properly targeted to LDs during their biogenesis, reinforcing the concept that Snx14 may assist in proper LD biogenesis by maintaining the lipid composition of ER sub-domains where LDs are generated [51]. None of these models are mutually exclusive, and further studies will be needed to understand the precise molecular role for Snx14 in organizing FA metabolism.

Snx14 is highly conserved in evolution, and related studies of Snx14 orthologs provide mechanistic insights into Snx14’s role in lipid homeostasis. *Drosophila* ortholog Snz functionally interacts with SCD1 ortholog DESAT1, and DESAT1 is required for the TG increases observed when Snz is over-expressed in fly adipose tissue [26]. Similarly, yeast ortholog Mdm1 functions in FA activation and LD biogenesis [25, 52]. As such, Mdm1-deficient yeast manifest sensitivity to high dosage of exogenous FAs, as well as altered ER morphology in their presence. Studies of both Snz and Mdm1 also indicate that these proteins localize to specific sub-regions of the ER network by virtue of their phospholipid-binding PX domains, which anchor them to other organelles and thereby help to demarcate ER sub-domains through their inter-organelle tethering capabilities. Thus, an intriguing possibility is that Snx14 family proteins act as organizational scaffolds of the ER network, and recruit enzymes into ER sub-domains to more efficiently process lipids.

Collectively, our observations provide a framework for understanding how Snx14 loss contributes to the cerebellar ataxia disease SCAR20. Indeed, a growing number

of genetic neurological diseases are attributed to loss of proteins which function in ER-localized lipid metabolism or in the maintenance of ER architecture [27-29]. Our data are consistent with a model where Snx14 loss perturbs the ability of cells to maintain proper FA metabolism and membrane lipid composition, ultimately elevating cellular SFA levels and/or saturated fatty acyl chains in organelle membranes. Such alterations may contribute to cellular lipotoxicity and the progressive death of neurons or other cell types, a pervasive symptom of SCAR20 disease [20, 22]. Though we focused our analysis here on the interplay between Snx14 and SCD1, the APEX2-based proteomics and lipidomics analysis will provide many insights in understanding the mechanisms behind SCAR20 pathology, as well as the further characterization of proteins at ER-LD contacts with roles in lipid metabolism.

Materials and Methods:

Cell culture

U2OS and HEK293 cells were maintained and expanded in DMEM (Corning, 10-013-CV) media containing 10% Cosmic Calf Serum (Hyclone, SH30087.04) and 1% Penicillin Streptomycin Solution (100X, Corning, 30-002-Cl). All cells were cultured at 37^{o}C and 5% CO_2. The cells were passaged with Trypsin-EDTA (Corning, 25-053-Cl) when they reach 80-90% confluency. For the cell viability assay, cells were treated with different concentration of FFA (250, 500, 750, 1000 uM) for 48 hours. For all other FFA treatment, the cells were incubated with 500uM of either OA or palmitate for the indicated period of time. In all the experiments the FFA were conjugated with fatty acid free BSA (Sigma, A3803) in the ratio of 6:1.

Chemicals and reagents

For cell treatments, the following reagents were used for indicated periods of time – 1) SCD inhibitor (Abcam, ab142089) - 4uM in DMSO (2) Myriocin (Sigma, M1177) – 50uM in DMSO (3) Tunicamycin (Sigma) – 5ug/ml in DMSO for 6hr (4) Etomoxir (Cayman chemical, 11969) – 10uM in DMSO (5) DGAT inhibitors include DGAT1 inhibitor (A-922500, Cayman chemical ,10012708) – 10uM in DMSO, and DGAT2 inhibitor (PF-06424439, Sigma, PZ0233)– 10uM in H_2O.

Generation of stable cell line

Stable cell line – U2OS cells stably expressing all C-terminally 3X Flag tagged $SNX14^{FL}$, $SNX14^{N}$ and $SNX14^{PXCN}$ generated in the previous study (ref) has been used here. Both $Snx14^{FLDTM}$ and $Snx14^{FLDPXA}$, with 3XFlag tag at the C-terminal, were generated following PCR amplification using $Snx14^{FL}$-3XFlag (primers available on request) and cloning into the plvx lentiviral vector with puromycin (puro) resistance cassette. Similarly GFP-Flag plasmid was cloned into plvx-puro vector. The cloned plasmids and lentiviral packaging plasmids were transfected together into 293T cells to generate lentivirus which were transduced into U2OS cells. Puromycin was used to select and expand the transduced cells expressing the

plasmid. The generated stable cell lines were stored in liquid nitrogen before their use in experiments.

Stable U2OS cells expressing Snx14^{EGFP}-APEX2 was used from (ref). Similar stable cell line generation method as described above was used to generate EGFP-APEX2-Sec61 which is also puromycin resistant. cDNA library was used for PCR amplification of Sec61. *SNX14*^{KO} *U2OS* cells used here was generated using CRISPR/Cas9 in (Datta, *JCB*, 2019).

Cloning and transient transfection

All C-terminally EGFP tagged Snx14 constructs i.e. SNX14^{FL}, SNX14^{N} and SNX14^{PXCN}, Snx14^{PX}, Snx14^{CN}, Snx14$^{PXCN\Box H}$, Snx14$^{FL\Box H}$ used were generated in (ref). Snx14-EGFP-APEX2 was cloned in pCMV vector for transient transfection. The primers used for cloning are available on request. HEK293 and U2OS cells were transiently transfected using PEI-Max Transfection reagent (Polysciences, 24765) and optimem (gibco, 31985-070) for 48 hours prior to experiments.

Cell viability assay

The cell viability assay protocol was adapted from [30, 31]. Cells were seeded at ~40% confluency and maintained in cell culture media overnight in a 12 well plate. On the following day, the cells were treated with indicated concentration of FFA for 2 days. Then the cells were washed with PBS, fixed with 4% PFA, stained with 0.1% crystal violet (Sigma) for 30 mins, excess stain was washed, and then the stain from the surviving cells were extracted with 10% acetic acid, whose optical density (OD) was measured at 600nm. The percentage of survival cells were quantified relative to the untreated cells whose OD measurement is set at 100% survival. The assay was performed thrice in triplicates.

Electron Microscopy

The U2OS cells were cultured under desired condition on MatTek dishes and processed in the UT Southwestern Electron Microscopy Core Facility. The cells were fixed with 2.5% (v/v) glutaraldehyde in 0.1M sodium cacodylate buffer, rinsed thrice in the buffer, and post-fixed in 1% osmium tetroxide and 0.8 % $K_3[Fe(CN_6)]$ in 0.1 M sodium cacodylate buffer at room temperature for 1 hr. After rinsing the fixed cells with water, they were en bloc stained with 2% aqueous uranyl acetate overnight. On the following day, the stained cells were rinsed in buffer and dehydrated with increasing concentration of ethanol. Next they were infiltrated with Embed-812 resin and polymerized overnight in a 60^{o}C oven. A diamond knife (Diatome) was used to section the blocks on a Leica Ultracut UCT (7) ultramicrotome (Leica Microsystems), which were collected onto copper grids, and post stained with 2% aqueous uranyl acetate and lead citrate. A Tecnai G^2 spirit transmission electron microscope (FEI) equipped with a LaB_6 source and a voltage of 120 kV was used to acquire the images.

Immunofluorescent staining and confocal imaging

For IF staining the cells were fixed with 4% PFA in PBS for 15-30 mins at room temperature. Then the cells were washed with PBS and permeabilized with 0.2% NP40 in PBS at RT for 3 mins. The cells were incubated with IF buffer (PBS containing 3% BSA, 0.1% NP40 and 0.02% sodium azide) for 40 mins to block non-specific binding. Next the cells were stained with primary antibody in IF buffer for 1 hr, washed with PBS thrice and stained with secondary antibody in IF buffer for 30 mins, again washed thrice with PBS, and used for imaging.

The primary antibodies used in this study are mouse anti-Hsp90B1 (1:300; Sigma, AMAb91019), rabbit anti-EGFP (1:300; Abcam, ab290), mouse anti-EGFP (1:200, Abcam, ab184601), rabbit anti-SCD1 (1:100; Abcam, ab39969), streptavidin-alexa 647 (Thermofisher Scientific, S21374). The secondary antibodies are donkey anti-mouse AF488 (Thermo Fisher, A21202) and donkey anti-rabbit AF594 (Thermo Fisher, A21207) used at a dilution of 1: 1000. LDs were stained with MDH (1:1000; Abgent, SM1000a) for 15 mins.

A Zeiss LSM 780 Confocal Microscope was used to acquire the images of the cells with a 63X oil immersion objective. Approx. 4-5 Z-sections of each image were taken. The images were merged by max z-projection.

Neutral lipid analysis by thin layer chromatography (TLC)

A protocol from [53] was used to extract lipids from cultured cells. Following treatment cells were washed twice with PBS, scraped and their pellet weights were detected. The pellets were treated with chloroform, methanol, 500 mM NaCl in 0.5% acetic acid such that the ratio of chloroform: methanol: water was 2:2:1.8. The suspended lysed cells were vortexed and centrifuged at 4000 rpm for 15 min at 4^{o}C. The bottom chloroform layer consisting of lipids was collected, dried and then resuspended in chloroform to a volume proportional to cell pellet weight. These lipids in chloroform were separated using thin layer chromatography (TLC). The solvent used to separate neutral lipids and FFAs was hexane: diethyl ether: acetic acid (80:20:1) or cyclohexane: ethylacetate (1:2). To develop the lipid spots, the TLC plates were sprayed with 3% copper acetate dissolved in 8% phosphoric acid and heated in the oven at 135°C for ~1hr. The spraying and heating of the TLC plates was repeated until the lipids could be properly visualized. Once the bands developed, the TLC plates were scanned and then Fiji (ImageJ) was used to quantify the intensity of the bands.

The relative change in intensity of each band was quantified with respect to untreated WT sample.

APEX2 dependent biotinylation

This protocol was modified from [39]. In brief, U2OS and HEK293 cells expressing APEX2 tagged constructs and non-APEX2 construct (negative control) were incubated with 500 uM biotin-phenol (BP) (Adipogen, CDX-B0270-M100) for 30 mins

and 1mM H2O2 was added for 1 min to biotinylate proteins proximal (labeling radius of ~20nm) to the expression of APEX2 tagged construct. The biotinylation reaction was quenched after 1 min by washing the cells thrice with a quencher solution (10mM sodium ascorbate, 5mM Trolox and 10mM sodium azide solution in DPBS).
To visualize the biotinylated proteins, the cells were IF-stained with streptavidin-alexa 647 (Thermofisher Scientific, S21374) during incubation with secondary antibody and then imaged using confocal miroscopy.
To identify the biotinylated proteins, immunoprecipitation and mass spectrometry techniques were used. After the labelling reaction, the cells were scraped in quencher solution and lysed RIPA lysis buffer consisting of protease inhibitor cocktail (ThermoFisher, 78430), 1mM PMSF and quenchers. The lysates were vortexed vigorously in cold for 30 mins and cleared by centrifuging at 10,000g for 10 mins at 4^{o}C. The cell lysate was then dialysed using Slide-A-Lyzer dialysis cassette (3500 MWCO, ThermoFisher Scientific) to remove unreacted free BP. The protein concentration was then measured using Pierce 660nm assay. 2 mg protein was incubated with 80ul streptavidin magnetic beads (Pierce, 88817) for 1 hour at room temperature on a rotator. The beads were pelleted using a magnetic rack. The pelleted beads were washed with a series of buffers - twice with RIPA lysis buffer, once with 1 M KCl, once with 0.1 M Na_2CO, once with 2 M urea solution in 10 mM Tris-HCl, pH 8.0, and twice with RIPA lysis buffer. To elute the biotinylated proteins , the beads were boiled in 80ul of 2X Laemmli Sample Buffer (Bio-Rad, 161-0737) supplemented with 2mM biotin and 20mM DTT. Some of the eluate was run in SDS page gel and Coomassie stained to visualize the amount of enriched protein. Some eluate was western blotted with streptavidin-HRP antibody to visualize protein biotinylation. The rest was processed for gel digestion and mass spectrometry (MS) analysis to identify the enriched biotinylated proteins.

Immunoprecipitation (IP)

To test co-IP of SCD1 with Snx14 constructs tagged with 3XFlag at the C-terminal, the cells expressing those Snx14 constructs were lysed with IPLB buffer (20mM HEPES, pH7.4, 150mM KOAc, 2mM Mg(Ac)2, 1mM EGTA, 0.6M Sorbitol,) supplemented with 1% w/v digitonin and protease inhibitor cocktail (PIC) (ThermoFisher, 78430), followed by pulse sonication. The lysate is clarified by centrifugation at 10,000g for 10 mins. 20ul of the supernatant was saved as the input. The rest of the supernatant was incubated with Flag M2 affinity gel (Sigma, A2220) for 2hrs at 4^{o}C. The beads were then washed thrice with IPLB wash buffer (IPLB, 0.1% digitonin, PIC) and twice with IPLB without digitonin. The IPed proteins are eluted from the beads by incubating the beads with 400ug/ml 3X Flag peptide in IPLB buffer for 30mins. The beads were spun down and the supernatant was collected. The supernantant and the input fraction was run in a SDS-page gel and western blotted for Flag constructs and SCD1.

Western blot

Whole cell lysate was prepared by scraping cultured cells, lysing them with RIPA lysis buffer containing protease inhibitor cocktail (ThermoFisher, 78430) and pulse sonication, and then clearing by centrifugation at 10,000g for 10 mins at 4^{o}C. Samples were prepared in 4X sample loading buffer containing 5% b-mercaptoethanol and boiled at 95^{0}C for 10 mins and then run on a 10% polyacrylamide gel. Wet transfer was run to transfer the proteins from the gel onto a PVDF membrane. The proteins on the membrane were probed by blocking the membrane with 5% milk in TBS-0.1%Tween (TBST) buffer for 1 hr at RT, incubating with primary antibodies overnight, washing with TBST thrice, incubating with HRP conjugated secondary antibodies (1:5000) and developing with Clarity™ Western ECL blotting substrate (Bio-Rad, 1705061) and imaging with X-ray film. The primary antibodies used for western blot were Rab anti-EGFP (1:2000), Mouse anti-Hsp90B1(1:1000), Mouse anti-Flag(1:1000), rabbit anti-SCD1 (1:500), guinea-pig PLIN3 (Progen, GP32), streptavidin-HRP (1:1000; Thermo Scientific, S911).
For quantitative densitometry, relative protein expression was quantified by analyzing band intensities using ImageJ (Fiji) and quantifying the fold change relative to untreated WT.

Lipid Analayiss Methods

Lipid analysis

All solvents were either HPLC or LC/MS grade and purchased from Sigma-Aldrich (St Louis, MO, USA). All lipid extractions were performed in 16×100mm glass tubes with PTFE-lined caps (Fisher Scientific, Pittsburg, PA, USA). Glass Pasteur pipettes and solvent-resistant plasticware pipette tips (Mettler-Toledo, Columbus, OH, USA) were used to minimize leaching of polymers and plasticizers. Fatty acid (FA) standards (FA(16:0{$^{2}H_{31}$}, FA(20:4ω6{$^{2}H_{8}$}) and FA(22:6ω3{$^{2}H_{5}$}) were purchased from Cayman Chemical (Ann Arbor, MI, USA), and used as internal standards for total fatty acid analysis by GC-MS. SPLASH Lipidomix (Avanti Polar Lipids, Alabaster, AL, USA) was used as internal standards for lipidomic analysis by LC-MS/MS.

Total Fatty Acid Analysis by GC-MS

Aliquots equivalent to 200k cells were transferred to fresh glass tubes for liquid-liquid extraction (LLE). The lipids were extracted by a three phase lipid extraction (3PLE) [54]. Briefly, 1mL of hexane, 1mL of methyl acetate, 0.75mL of acetonitrile, and 1mL of water was added to the glass tube containing the sample. The mixture was vortexed for 5 seconds and then centrifuged at 2671×*g* for 5 min, resulting in separation of three distinct liquid phases. The upper (UP) and middle (MID) organic phases layers were collected into separate glass tubes and dried under N_2. The dried extracts were resuspended in 1mL of 0.5M potassium hydroxide solution prepared in methanol, spiked with fatty acid internal standards, and hydrolyzed at 80°C during 60 minutes. Hydrolyzed fatty acids were extracted by adding 1mL each of dichloromethane and water to the sample in hydrolysis solution. The mixture was vortexed and centrifuged at 2671×*g* for 5 minutes, and the organic phase was

collected to a fresh glass tube and dried under N_2. Total fatty acid profiles were generated by a modified GC-MS method previously described by *[55]*. Briefly, dried extracts were resuspendend in 50µL of 1% triethylamine in acetone, and derivatized with 50µL of 1% pentafluorobenzyl bromide (PFBBr) in acetone at room temperature for 25 min in capped glass tubes. Solvents were dried under N_2, and samples were resuspended in 500µL of isooctane. Samples were analyzed using an Agilent 7890/5975C (Santa Clara, CA, USA) by electron capture negative ionization (ECNI) equipped with a DB-5MS column (40m x 0.180mm with 0.18µm film thickness) from Agilent. Hydrogen was used as carrier gas and injection port temperature were set at 300°C. Fatty acids were analyzed in selected ion monotoring (SIM) mode. The FA data was normalized to the internal standards. Fatty acid with carbon length; C ≤ 18 were normalized to FA(16:0{$^2H_{31}$}), C = 20 were normalized to FA(20:4 ω6{$^2H_8$}), and C = 22 were normalized to FA(22:6 ω3{$^2H_5$}). Data was processed using MassHunter software (Agilent). Abundance of lipids in each of the samples are normalized to cell number.

Lipidomic analysis by LC-MS/MS

Aliquots equivalent to 200k cells were transferred to fresh glass tubes for LLE. Samples were dried under N_2 and extracted by Bligh/Dyer [56]; 1mL each of dichloromethane, methanol, and water were added to a glass tube containing the sample. The mixture was vortexed and centrifuged at 2671×*g* for 5 min, resulting in two distinct liquid phases. The organic phase was collected to a fresh glass tube, spiked with internal standards and dried under N_2. Samples were resuspendend in Hexane.

Lipids were analyzed by LC-MS/MS using a SCIEX QTRAP 6500$^+$ equipped with a Shimadzu LC-30AD (Kyoto, Japan) HPLC system and a 150 × 2.1 mm, 5µm Supelco Ascentis silica column (Bellefonte, PA, USA). Samples were injected at a flow rate of 0.3 ml/min at 2.5% solvent B (methyl tert-butyl ether) and 97.5% Solvent A (hexane). Solvent B is increased to 5% during 3 minutes and then to 60% over 6 minutes. Solvent B is decreased to 0% during 30 seconds while Solvent C (90:10 (v/v) Isopropanol-water) is set at 20% and increased to 40% during the following 11 minutes. Solvent C is increased to 44% for 6 minutes and then to 60% during 50 seconds. The system was held at 60% of solvent C during 1 minutes prior to re-equilibration at 2.5% of solvent B for 5 minutes at a 1.2mL/min flow rate. Solvent D (95:5 (v/v) Acetonitrile-water with 10mM Ammonium acetate) was infused post-column at 0.03ml/min. Column oven temperature was 25°C). Data was acquired in positive and negative ionization mode using multiple reaction monitoring (MRM). Each lipid class was normalized to its correspondent internal standard. The LC-MS data was analyzed using MultiQuant software (SCIEX). Abundance of lipids in each of the samples are normalized to cell number.

Acknowledgements

The authors would like to thank Joel Goodman, Sandra Schmid, Russell Debose-Boyd, and members of the Henne lab for help and conceptual advise in the completion of this study. We would also like to thank Dr. Philip Stanier and Dr. Dale Bryant (UCL, London, UK) for providing the SCAR20 patient-derived cells. We acknowledge Dr. Kate Luby-Phelps and Anza Darehshouri for technical assistance with confocal and electron microscopy. We thank Dr. Andrew Lemoff for assistance with mass-spectrometry proteomics. W.M.H. is supported by funds from the Welch Foundation (I-1873), the Searle Foundation (SSP-2016-1482), the NIH NIGMS (GM119768), and the UT Southwestern Endowed Scholars Program. S.D. is supported by an AHA Pre-doctoral Fellowship Grant (20PRE35210230). JGM is supported in part by NIH 2 PO1 HL20948-33 grants.

Figure legends:

Figure 1: Snx14 deficient cells are hypersensitive to saturated fatty acids

A. Percentage of surviving cells denoted as cell viability (%) of WT and *SNX14*^{KO} cells, following treatment with increasing concentration (0, 250, 500, 750, 1000mM) of palmitoleate (FA|16:1) for 2 days. A'. Treatment of WT and *SNX14*^{KO} cells with similar increasing concentration of oleate (FA|18:1) for 2 days. The assay was repeated thrice in triplicates. Values represent mean±SEM. Signiificance test between WT and *SNX14*^{KO} (n=3, ***p<0.0001,**p<0.001,*p<0.01, multiple t-test by Holm-Sidak method with alpha = 0.05)

B. Cell viability (%) of WT and *SNX14*^{KO} cells, showing *SNX14*^{KO} cells are hypersensitive following addition of increasing concentration (0, 250, 500, 750, 1000uM) of palmitate (FA|16:0) for 2 days. B'. Exposure to similar increasing concentration of stereate (FA|18:0) for 2 days in WT and *SNX14*^{KO} cells. The assay was repeated thrice in triplicates. Values represent mean±SEM (n=3, **p<0.001, multiple t-test by Holm-Sidak method with alpha = 0.05)

C. Cell viability of fibroblasts derived from 2 WT and 1 SCAR20/Snx14^{Mut} patients, showing hypersensitivity of SCAR20 cells following 2-day exposure to 0, 1000, 2000uM palmitate. The assay was repeated thrice in triplicates. Values represent mean±SEM (n=3, *p<0.01 reltive to WT-1, $^{\#\#}$p<0.001 and $^{\#\#\#}$p<0.0001 relative to WT-2, multiple t-test by Holm-Sidak method with alpha = 0.05)

D. Cell viability of WT and *SNX14*^{KO} cells treated with 10uM Etomoxir along with increasing palmitate concentration (0, 250, 500, 750, 1000uM) for 2 days.

E. Cell viability of WT and *SNX14*^{KO} cells following addition of increasing palmitate concentration (0, 250, 500, 750, 1000uM) in presence of 50uM Myriocin for 2 days. The assay was repeated thrice in triplicates. Values represent mean±SEM.

Figure 2: Palmitate-induced hypersensitivity in *SNX14*^{KO} is associated with defective ER morphology

A. Immunofluorescent (IF) labeling of the ER with a-HSP90B1 (ER marker) antibody before and after overnight palmitate treatment in WT and *SNX14*^{KO} cells. Scale bar = 10μm

B. TEM micrographs of WT and *SNX14*^{KO} cells with no palmitate treatment and with palmitate treatment for 6hr and overnight to visualize ER ultra-structure. Scale bar = 1μm. Scale bar of inset = 0.5 μm

Figure 3: APEX2-based proteomics reveals the Snx14-associated ER-LD proteome

A. Schematic diagram showing Snx14 tagged with EGFP followed by APEX2 at the C-terminus. The reaction of biotin phenol and H2O2 catalysed by APEX2 generates biotin-phenoxyl radicals which covalently attaches with proteins in proximity of ~20nm from Snx14. Following OA treatment, APEX2 tagged Snx14 enriches at ER-LD contacts and hence the labelling reaction is expected to biotinylate the interactors of Snx14 at those contacts.

B. Co-IF staining of cells stably expressing Snx14-EGFP-APEX2 with anti-EGFP (green) antibody, streptavidin-Alexa647 fluorophore (biotinylated proteins, red) and LDs staining with monodansylpentane (MDH, blue) and confocal imaging revealed colocalization of Snx14 and biotinylated proteins surrounding LDs. Scale bar = 10μm

C. Biotinylated proteins pulled down by streptavidin conjugated beads from Snx14-EGFP-APEX2 and no-APEX2 (negative control) expressing HEK293 and U2OS cells were coomassie stained. Western blotting of the same pulled down lysates with streptavidin-HRP antibody revealed biotinylation of several proteins in Snx14-EGFP-APEX2 relative to the negative control.

D. Venn diagram representing the multi-stage analysis of the Mass spectrometry data which identified protein abundance in Snx14-EGFP-APEX2, no-APEX2 and EGFP-APEX2-Sec61. 2241 proteins are enriched >2 fold in Snx14-EGFP-APEX2 (1: purple circle). Among them 674 which are also enriched in APEX2 tagged Sec61are excluded (2 : black circle). 311 of (1) are ER-associated according to Gene ontology analysis (3: red circle). Again 305 of (1) comprise of genes deletion of which cause sensitivity to palmitate according to a CRISPR/Cas9 screen [40] (4 : yellow circle). Overlap of sets (1),(3) and (4) consist of 29 ER-associated proteins which are enriched for Snx14 and important for palmitate

metabolism. These set of Snx14 interactome are compared with its fly homolog Snz interactome.

E. Proteins enriched for Snx14 from set (1) of Fig D after excluding proteins also enriched for Sec61 are plotted from HEK293 and U2OS cells as log_2 fold enrichment relative to negative control and are denoted by grey dots. Orange dots represent those proteins whose CRISPR/Cas9 deletion results in palmitate mediated sensitivity.

F. Gene ontology enrichment analysis by ClueGO using Cytoscape software clustered genes from set (1) of Fig D according to their association with a cellular organelle.

Supplementary Figure 3

A. Log_2 fold enrichment of proteins in APEX2-Sec61 relative to negative control from HEK293 and U2OS cells are plotted denoted by grey dots.

B. Examples of some proteins including LD-associated proteins which are specifically enriched in Snx14 after analysis in Fig 3D and also has a high negative screen score showing palmitate sensitivity to similar to Snx14 from [40]

C. Frequency distribution of the CRISPR/Cas9 screened genes tested negative (<-1.8) for palmitate treatment from [40] enriched specifically for Snx14 (denoted as orange dots) in Fig 3E.

D. Gene ontology enrichment analysis by ClueGO using Cytoscape software clustered ER-localized genes from Fig 3F according to their molecular function.

Figure 4: ER association of Snx14 is necessary for its SCD1 interaction

A. Western blotting with anti-Flag and anti-SCD1 antibody of 2% input lysate from GFP-Flag and Snx14-Flag expressing cells with and without palmitate treatment reveals relative expression of GFP-Flag, Snx14-Flag and SCD1 (upper band). Co-immunoprecipitation (Co-IP) of SCD1 with Flag tagged constructs reveals presence of SCD1 in Snx14-Flag and not GFP-Flag enriched beads when western blotted with anti-Flag and anti-SCD1 antibody.

B. Schematic diagram of Snx14 fragments C-terminally tagged with either 3X Flag or EGFP. $Snx14^{FL}$ depicts the full length human Snx14. $Snx14^{N}$ is the N-terminal fragment that spans from the beginning and includes PXA and RGS domains. $Snx14^{PXCN}$ is the Ce-terminal half including the PX domain and C-Nexin domains.

C. Lanes represent 2% input and IP from GFP-Flag, all 3XFlag tagged Snx14 constructs ($Snx14^{FL}$, $Snx14^{N}$, $Snx14^{PXCN}$) and SCD1 inhibitor treated $Snx14^{FL}$-3XFlag expressing U2OS cells. Western blotting with anti-Flag and anti-SCD1

antibody reveals relative expression of all the Flag tagged constructs and SCD1 in all these samples. Among all the samples, $Snx14^{FL}$ in presence of SCD1 inhibitor and $Snx14^{N}$ could co-IP SCD1 similar to $Snx14^{FL}$.

D. IF staining of WT cells and cells expressing $Snx14^{FL}$, $Snx14^{N}$, $Snx14^{PXCN}$ with anti-EGFP(green), anti-SCD1(gray) antibody and imaged with confocal microscope. LDs were stained with MDH (blue). All cells were treated with OA. Scale bar = 10 µm.

Supplementary Figure 4

A. Lanes represent 2% input and IP from GFP-Flag and $Snx14^{FL}$-3XFlag expressing U2OS cells with oleate and palmitate treatment respectively. Western blotting with anti-Flag and anti-PLIN3 antibody reveals relative expression of all the Flag tagged constructs and PLIN3 in all these samples. $Snx14^{FL}$-3XFlag similar to GFP-Flag could not co-IP PLIN3.

B. IF staining of WT cells and cells expressing $Snx14^{FL}$, $Snx14^{N}$, $Snx14^{PXCN}$ with anti-EGFP(green), anti-SCD1(red) antibody and imaged with confocal microscope. LDs were stained with MDH (blue). All cells were treated with OA. Scale bar = 10 µm.

Figure 5: SCD1 can rescue *SNX14*^{KO} palmitate-induced lipotoxicity

A. Western blot of SCD1 and Hsp90B1 (ER marker) before and after overnight palmitate treatment in WT, *SNX14*^{KO} and Snx14FlagO/E cells.

B. Ratio of the intensity of the protein bands of SCD1 over Hsp90B1 are quantified from Fig 5A, and plotted as fold change relative to untreated WT whose ratio is set as 1. Values represent mean±SEM. Significance test between before and after palmitate treatment denoted as # (n=3, $^{\#}p<0.1$, $^{\#\#}p<0.001$, multiple t-test by Holm-Sidak method with alpha = 0.05). Significance test between WT, *SNX14*^{KO} and Snx14FlagO/E is denoted as *(n=3, *p<0.01, multiple t-test by Holm-Sidak method with alpha = 0.05)

C. Cell viability (%) of WT and *SNX14*^{KO} cells, showing sensitivity of both WT and *SNX14*^{KO} cells are rescued with overexpression of SCD1 following addition of increasing concentration (0, 500, 750, 1000uM) of palmitate for 2 days. The assay was repeated thrice in triplicates. Values represent mean±SEM. Significance test between WT and WT+SCD1 denoted as * (n=3, **p<0.001, ***p<0.0001, multiple t-test by Holm-Sidak method with alpha = 0.05) Significance test between *SNX14*^{KO} and *SNX14*^{KO} +SCD1 denoted as $^{\#}$ (n=3, $^{\#\#}p<0.001$, $^{\#\#}$ p<0.0001,multiple t-test by Holm-Sidak method with alpha = 0.05).

D. Cell viability shows increase in surviving WT and *SNX14*^{KO} cells when treatment with 1mM palmitate is supplemented with 100 and 200uM of OA. The assay was repeated thrice in triplicates. Values represent mean±SEM (**p<0.001, multiple t-test by Holm-Sidak method with alpha = 0.05, significance test between oleate treatment with non-oleate treatment)

E. Cell viability (%) of WT and *SNX14*^{KO} cells, showing sensitivity of both WT and *SNX14*^{KO} cells are reduced with reintroduction of SCD1 in presence of DGAT1/2 inhibitors following addition of increasing concentration (0, 500, 750, 1000uM) of palmitate for 2 days. The assay was repeated thrice in triplicates. Values represent mean±SEM. Significance test between WT and WT+SCD1denoted as * (n=3, *p<0.01, **p<0.001, ***p<0.0001, multiple t-test by Holm-Sidak method with alpha = 0.05) Significance test between *SNX14*^{KO} and *SNX14*^{KO} +SCD1 denoted as $^{\#}$ (n=3, $^{\#\#}$p<0.001, $^{\#\#}$ p<0.0001, multiple t-test by Holm-Sidak method with alpha = 0.05).

F. Cell death (%) after exposure to 500uM of palmitate in WT, *SNX14*^{KO}, and on re-addition of empty vector (EV), Snx14^{FL}, Snx14^{N}, Snx14^{PXCN}, Snx14^{FLDTM}, Snx14^{FLDPXA}. Values represent mean±SEM. Significance test compared with WT is denoted as * (n=3, *p<0.001, multiple t-test analysis by Holm-Sidak method with alpha = 0.05.

G. Schematic diagram of Snx14 fragments C-terminally tagged with 3X Flag. Snx14^{FL} depicts the full length human Snx14. Snx14 ^{FLDPXA} and Snx14 ^{FLDTM} are the full length Snx14 excluding the PXA domain and TM domain respectively.

H. Lanes represent 2% input and IP from GFP-Flag, 3XFlag tagged Snx14 constructs (Snx14^{FL}, Snx14^{FLDPXA}, Snx14^{FLDTM}) expressing U2OS cells. Western blotting with anti-Flag and anti-SCD1 antibody reveals relative expression of all the Flag tagged constructs and SCD1 in all these samples. Snx14^{FLDPXA} could co-IP SCD1 similar to Snx14^{FL} whereas Snx14^{FLDTM} could not pull down SCD1.

Supplementary Figure 5

A. Cell viability of WT and *SNX14*^{KO} cells treated with 4uM SCDi along with increasing palmitate concentration (0, 250, 500uM) for 2 days. D'. The assay was repeated thrice in triplicates. Values represent mean±SEM. (n=3, **p<0.001, multiple t-test by Holm-Sidak method with alpha = 0.05)

Figure 6: *SNX14*^{KO} cells have defective FA processing which can be rescued by SCD1 over-expression

A. TLC of neutral lipids and FFAs in WT and *SNX14*^{KO} cells treated with 500uM palmitate for 0, 2, 4, 8, 16 hours. A' Quantification of relative fold change in FFA (normalized to cell pellet weight) with respect to untreated WT of TLC from A. Values represent mean±SEM (n=3, *p<0.01, multiple t-test by Holm-Sidak method with alpha = 0.05).

B. TLC of neutral lipids and FFAs in WT and *SNX14*^{KO} cells before and after overexpression of SCD1 treated following exposure to 500uM palmitate for 0, 4, 16 hours. B' Quantification of relative fold change in FFA (normalized to cell pellet weight) with respect to untreated WT of TLC from B. Values represent mean±SEM (n=2, *p<0.01, **p<0.001, multiple t-test by Holm-Sidak method with alpha = 0.05).

C. Immunofluorescent (IF) labeling of the ER with a-HSP90B1 (ER marker) antibody in *SNX14*^{KO} cells before and after overexpression of SCD1 following overnight palmitate treatment. Scale bar = 10mm.

D. Abundance of FAs (16:0) derived from phospholipids of WT and *SNX14*^{KO} cells relative to untreated WT under the following conditions – no treatment, palmitate treatment and treatment with palmitate and SCD1 inhibitor. Values represent mean±SEM (n=3, *p<0.01, multiple t-test by Holm-Sidak method with alpha = 0.05).

Supplementary Figure 6

A. Abundance of all fatty acids derived from phospholipids of WT and *SNX14*^{KO} cells relative to untreated WT under the following conditions – no treatment, palmitate treatment and treatment with palmitate and SCD1 inhibitor. Values represent mean±SEM (n=3, *p<0.01, multiple t-test by Holm-Sidak method with alpha = 0.05).

Figure 7: Lipidomic profiling reveals that *SNX14*^{KO} cells display enhanced saturated lipid composition that mimics SCD1 inhibition

A. Heatmap indicating the relative change in abundance of individual lipid species of *U2OS* WT and *SNX14*^{KO} cells before and after palmitate treatment relative to untreated WT cells.

B. Heatmap indicating the relative change in abundance of 60 different TG species of WT and *SNX14*^{KO} cells relative to untreated WT. These cells were either untreated or treated with palmitate or palmitate in presence of SCD1 inhibitor. The label N indicates the number of double bonds in those group of TG species. The vertical serial number represents a different TG species where 1 is

TG|50:0|(NL-16:0) and 11 is TG|48:1|(NL-16:1) and they exhibit the most changes in TG in the treated *SNX14*^{KO} cells.

C. Abundance of TG (with 0 or 1 unsaturation) relative to untreated WT as analyzed in WT and *SNX14*^{KO} cells. Prior to lipid extraction and lipidomics, these cells were either untreated or treated with palmitate and palmitate in presence of SCD1 inhibitor. Values represent mean±SEM (n=3, *p<0.01, multiple t-test by Holm-Sidak method with alpha = 0.05).

D. Heatmap indicating the relative change in abundance of 9 different LPC species of WT and *SNX14*^{KO} cells relative to untreated WT. These cells were either untreated or treated with palmitate and palmitate in presence of SCD1 inhibitor.

Supplementary Figure 7

A. Heatmap indicating the relative change in abundance of 5 different LPE species of WT and *SNX14*^{KO} cells relative to untreated WT. These cells were either untreated or treated with palmitate and palmitate in presence of SCD1 inhibitor.

B. Heatmap indicating the relative change in abundance of 7 different PC species of WT and *SNX14*^{KO} cells relative to untreated WT. These cells were either untreated or treated with palmitate and palmitate in presence of SCD1 inhibitor.

C. Heatmap indicating the relative change in abundance of 24 different PS species of WT and *SNX14*^{KO} cells relative to untreated WT. These cells were either untreated or treated with palmitate and palmitate in presence of SCD1 inhibitor.

Figure 8 : Working Model for Snx14 in maintaining cellular lipid composition

Working model for Snx14 in maintaining ER lipid homeostasis when challenged with excess SFAs. WT and *SNX14*^{KO} cells are displayed. – (1) Interaction of Snx14 and SCD1 converts SFAs to MUFAs, (2) Integration of both SFAs and MUFAs into polar and neutral lipids helps to balancea lipid saturation and maintain cellular lipid homeostasis. Snx14, via its N-terminal region, interacts with SCD1 and also binds to growing LDs via its C-terminal C-Nexin domain to functionally connect FA processing to LD biogenesis. (3) Snx14 loss results in SFA accumulation and a defect in processing SFAs at sites adjacent to LD bud sites (4) Excess SFAs eventually integrate into polar lipids, increasing saturated lipid content in TG, PC, and PS. Lysolipids such as LPC and LPE also accumulate and contain elevated saturated acyl chains. Simultaneously, SCD1 protein level increase, but still fail to properly maintain lipid homeostasis. Altogether, ER morphology is compromised eventually causing lipotoxicity and cell death. This SFA accumulation and cell death can be rescued by ectopic expression of SCD1.

References

1. Schaffer, J.E., *Lipotoxicity: when tissues overeat.* Curr Opin Lipidol, 2003. **14**(3): p. 281-7.
2. Lelliott, C. and A.J. Vidal-Puig, *Lipotoxicity, an imbalance between lipogenesis de novo and fatty acid oxidation.* Int J Obes Relat Metab Disord, 2004. **28 Suppl 4**: p. S22-8.
3. Ertunc, M.E. and G.S. Hotamisligil, *Lipid signaling and lipotoxicity in metaflammation: indications for metabolic disease pathogenesis and treatment.* J Lipid Res, 2016. **57**(12): p. 2099-2114.
4. Kusminski, C.M., et al., *Diabetes and apoptosis: lipotoxicity.* Apoptosis, 2009. **14**(12): p. 1484-95.
5. Ye, R., T. Onodera, and P.E. Scherer, *Lipotoxicity and beta Cell Maintenance in Obesity and Type 2 Diabetes.* J Endocr Soc, 2019. **3**(3): p. 617-631.
6. Borradaile, N.M. and J.E. Schaffer, *Lipotoxicity in the heart.* Curr Hypertens Rep, 2005. **7**(6): p. 412-7.
7. Schaffer, J.E., *Lipotoxicity: Many Roads to Cell Dysfunction and Cell Death: Introduction to a Thematic Review Series.* J Lipid Res, 2016. **57**(8): p. 1327-8.
8. Bruce, K.D., A. Zsombok, and R.H. Eckel, *Lipid Processing in the Brain: A Key Regulator of Systemic Metabolism.* Front Endocrinol (Lausanne), 2017. **8**: p. 60.
9. Estadella, D., et al., *Lipotoxicity: effects of dietary saturated and transfatty acids.* Mediators Inflamm, 2013. **2013**: p. 137579.
10. Piccolis, M., et al., *Probing the Global Cellular Responses to Lipotoxicity Caused by Saturated Fatty Acids.* Mol Cell, 2019. **74**(1): p. 32-44 e8.
11. Hetherington, A.M., et al., *Differential Lipotoxic Effects of Palmitate and Oleate in Activated Human Hepatic Stellate Cells and Epithelial Hepatoma Cells.* Cell Physiol Biochem, 2016. **39**(4): p. 1648-62.
12. Borradaile, N.M., et al., *Disruption of endoplasmic reticulum structure and integrity in lipotoxic cell death.* J Lipid Res, 2006. **47**(12): p. 2726-37.
13. Listenberger, L.L., et al., *Triglyceride accumulation protects against fatty acid-induced lipotoxicity.* Proc Natl Acad Sci U S A, 2003. **100**(6): p. 3077-82.
14. Fujimoto, T. and R.G. Parton, *Not just fat: the structure and function of the lipid droplet.* Cold Spring Harb Perspect Biol, 2011. **3**(3).
15. Plotz, T., et al., *The role of lipid droplet formation in the protection of unsaturated fatty acids against palmitic acid induced lipotoxicity to rat insulin-producing cells.* Nutr Metab (Lond), 2016. **13**: p. 16.
16. Wilfling, F., et al., *Triacylglycerol synthesis enzymes mediate lipid droplet growth by relocalizing from the ER to lipid droplets.* Dev Cell, 2013. **24**(4): p. 384-99.
17. Szymanski, K.M., et al., *The lipodystrophy protein seipin is found at endoplasmic reticulum lipid droplet junctions and is important for droplet morphology.* Proc Natl Acad Sci U S A, 2007. **104**(52): p. 20890-5.
18. Salo, V.T., et al., *Seipin Facilitates Triglyceride Flow to Lipid Droplet and Counteracts Droplet Ripening via Endoplasmic Reticulum Contact.* Dev Cell, 2019. **50**(4): p. 478-493 e9.
19. Xu, N., et al., *The FATP1-DGAT2 complex facilitates lipid droplet expansion at the ER-lipid droplet interface.* J Cell Biol, 2012. **198**(5): p. 895-911.

20. Thomas, A.C., et al., *Mutations in SNX14 cause a distinctive autosomal-recessive cerebellar ataxia and intellectual disability syndrome.* Am J Hum Genet, 2014. **95**(5): p. 611-21.
21. Shukla, A., et al., *Autosomal recessive spinocerebellar ataxia 20: Report of a new patient and review of literature.* Eur J Med Genet, 2017. **60**(2): p. 118-123.
22. Akizu, N., et al., *Biallelic mutations in SNX14 cause a syndromic form of cerebellar atrophy and lysosome-autophagosome dysfunction.* Nat Genet, 2015. **47**(5): p. 528-34.
23. Datta, S., et al., *Cerebellar ataxia disease-associated Snx14 promotes lipid droplet growth at ER-droplet contacts.* J Cell Biol, 2019. **218**(4): p. 1335-1351.
24. Bryant, D., et al., *SNX14 mutations affect endoplasmic reticulum-associated neutral lipid metabolism in autosomal recessive spinocerebellar ataxia 20.* Hum Mol Genet, 2018. **27**(11): p. 1927-1940.
25. Hariri, H., et al., *Mdm1 maintains endoplasmic reticulum homeostasis by spatially regulating lipid droplet biogenesis.* J Cell Biol, 2019. **218**(4): p. 1319-1334.
26. Ugrankar, R., et al., *Drosophila Snazarus Regulates a Lipid Droplet Population at Plasma Membrane-Droplet Contacts in Adipocytes.* Dev Cell, 2019. **50**(5): p. 557-572 e5.
27. Blackstone, C., C.J. O'Kane, and E. Reid, *Hereditary spastic paraplegias: membrane traffic and the motor pathway.* Nat Rev Neurosci, 2011. **12**(1): p. 31-42.
28. Yamanaka, T. and N. Nukina, *ER Dynamics and Derangement in Neurological Diseases.* Front Neurosci, 2018. **12**: p. 91.
29. Adibhatla, R.M. and J.F. Hatcher, *Altered lipid metabolism in brain injury and disorders.* Subcell Biochem, 2008. **49**: p. 241-68.
30. Feoktistova, M., P. Geserick, and M. Leverkus, *Crystal Violet Assay for Determining Viability of Cultured Cells.* Cold Spring Harb Protoc, 2016. **2016**(4): p. pdb prot087379.
31. Chu, B.B., et al., *Cholesterol transport through lysosome-peroxisome membrane contacts.* Cell, 2015. **161**(2): p. 291-306.
32. Spigoni, V., et al., *Stearic acid at physiologic concentrations induces in vitro lipotoxicity in circulating angiogenic cells.* Atherosclerosis, 2017. **265**: p. 162-171.
33. Turpin, S.M., et al., *Apoptosis in skeletal muscle myotubes is induced by ceramides and is positively related to insulin resistance.* Am J Physiol Endocrinol Metab, 2006. **291**(6): p. E1341-50.
34. Ellingson, J.S., E.E. Hill, and W.E. Lands, *The control of fatty acid composition in glycerolipids of the endoplasmic reticulum.* Biochim Biophys Acta, 1970. **196**(2): p. 176-92.
35. Bell, R.M. and R.A. Coleman, *Enzymes of glycerolipid synthesis in eukaryotes.* Annu Rev Biochem, 1980. **49**: p. 459-87.
36. Schrauwen, P., et al., *Mitochondrial dysfunction and lipotoxicity.* Biochim Biophys Acta, 2010. **1801**(3): p. 266-71.
37. Haffar, T., F. Berube-Simard, and N. Bousette, *Impaired fatty acid oxidation as a cause for lipotoxicity in cardiomyocytes.* Biochem Biophys Res Commun, 2015. **468**(1-2): p. 73-8.
38. Shen, Y., et al., *Metabolic activity induces membrane phase separation in endoplasmic reticulum.* Proc Natl Acad Sci U S A, 2017. **114**(51): p. 13394-13399.

39. Hung, V., et al., *Spatially resolved proteomic mapping in living cells with the engineered peroxidase APEX2.* Nat Protoc, 2016. **11**(3): p. 456-75.
40. Zhu, X.G., et al., *CHP1 Regulates Compartmentalized Glycerolipid Synthesis by Activating GPAT4.* Mol Cell, 2019. **74**(1): p. 45-58 e7.
41. Paton, C.M. and J.M. Ntambi, *Biochemical and physiological function of stearoyl-CoA desaturase.* Am J Physiol Endocrinol Metab, 2009. **297**(1): p. E28-37.
42. Miyazaki, M., et al., *The biosynthesis of hepatic cholesterol esters and triglycerides is impaired in mice with a disruption of the gene for stearoyl-CoA desaturase 1.* J Biol Chem, 2000. **275**(39): p. 30132-8.
43. Miyazaki, M., Y.C. Kim, and J.M. Ntambi, *A lipogenic diet in mice with a disruption of the stearoyl-CoA desaturase 1 gene reveals a stringent requirement of endogenous monounsaturated fatty acids for triglyceride synthesis.* J Lipid Res, 2001. **42**(7): p. 1018-24.
44. Uto, Y., et al., *Discovery of novel SCD1 inhibitors: 5-alkyl-4,5-dihydro-3H-spiro[1,5-benzoxazepine-2,4'-piperidine] analogs.* Eur J Med Chem, 2011. **46**(5): p. 1892-6.
45. Ntambi, J.M. and M. Miyazaki, *Regulation of stearoyl-CoA desaturases and role in metabolism.* Prog Lipid Res, 2004. **43**(2): p. 91-104.
46. Olzmann, J.A. and P. Carvalho, *Dynamics and functions of lipid droplets.* Nat Rev Mol Cell Biol, 2019. **20**(3): p. 137-155.
47. Liu, X., M.S. Strable, and J.M. Ntambi, *Stearoyl CoA desaturase 1: role in cellular inflammation and stress.* Adv Nutr, 2011. **2**(1): p. 15-22.
48. Matsui, H., et al., *Stearoyl-CoA desaturase-1 (SCD1) augments saturated fatty acid-induced lipid accumulation and inhibits apoptosis in cardiac myocytes.* PLoS One, 2012. **7**(3): p. e33283.
49. Ralston, J.C., et al., *SCD1 mediates the influence of exogenous saturated and monounsaturated fatty acids in adipocytes: Effects on cellular stress, inflammatory markers and fatty acid elongation.* J Nutr Biochem, 2016. **27**: p. 241-8.
50. Bersuker, K., et al., *A Proximity Labeling Strategy Provides Insights into the Composition and Dynamics of Lipid Droplet Proteomes.* Dev Cell, 2018. **44**(1): p. 97-112 e7.
51. Cao, Z., et al., *Dietary fatty acids promote lipid droplet diversity through seipin enrichment in an ER subdomain.* Nat Commun, 2019. **10**(1): p. 2902.
52. Hariri, H., et al., *Lipid droplet biogenesis is spatially coordinated at ER-vacuole contacts under nutritional stress.* EMBO Rep, 2018. **19**(1): p. 57-72.
53. Bligh, E.G. and W.J. Dyer, *A rapid method of total lipid extraction and purification.* Can J Biochem Physiol, 1959. **37**(8): p. 911-7.
54. Vale, G., et al., *Three-phase liquid extraction: a simple and fast method for lipidomic workflows.* J Lipid Res, 2019. **60**(3): p. 694-706.
55. Quehenberger, O., A.M. Armando, and E.A. Dennis, *High sensitivity quantitative lipidomics analysis of fatty acids in biological samples by gas chromatography-mass spectrometry.* Biochim Biophys Acta, 2011. **1811**(11): p. 648-56.
56. Blight, E.G. and W.J. Dyer, *A rapid method of total lipid extraction and purification.* Canadian Journal of Biochemistry and Physiology, 1959. **37**: p. 911-917.

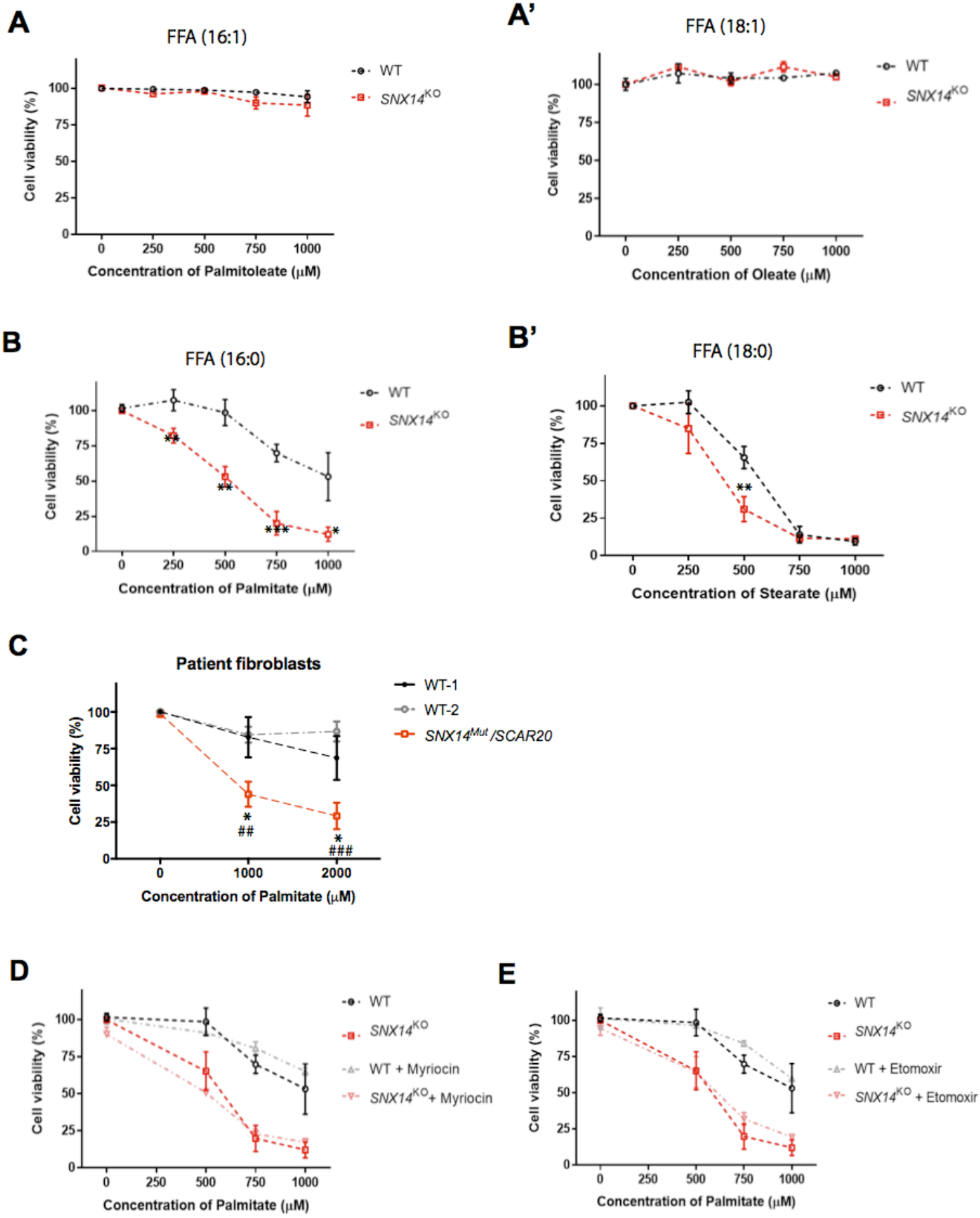

Figure 1

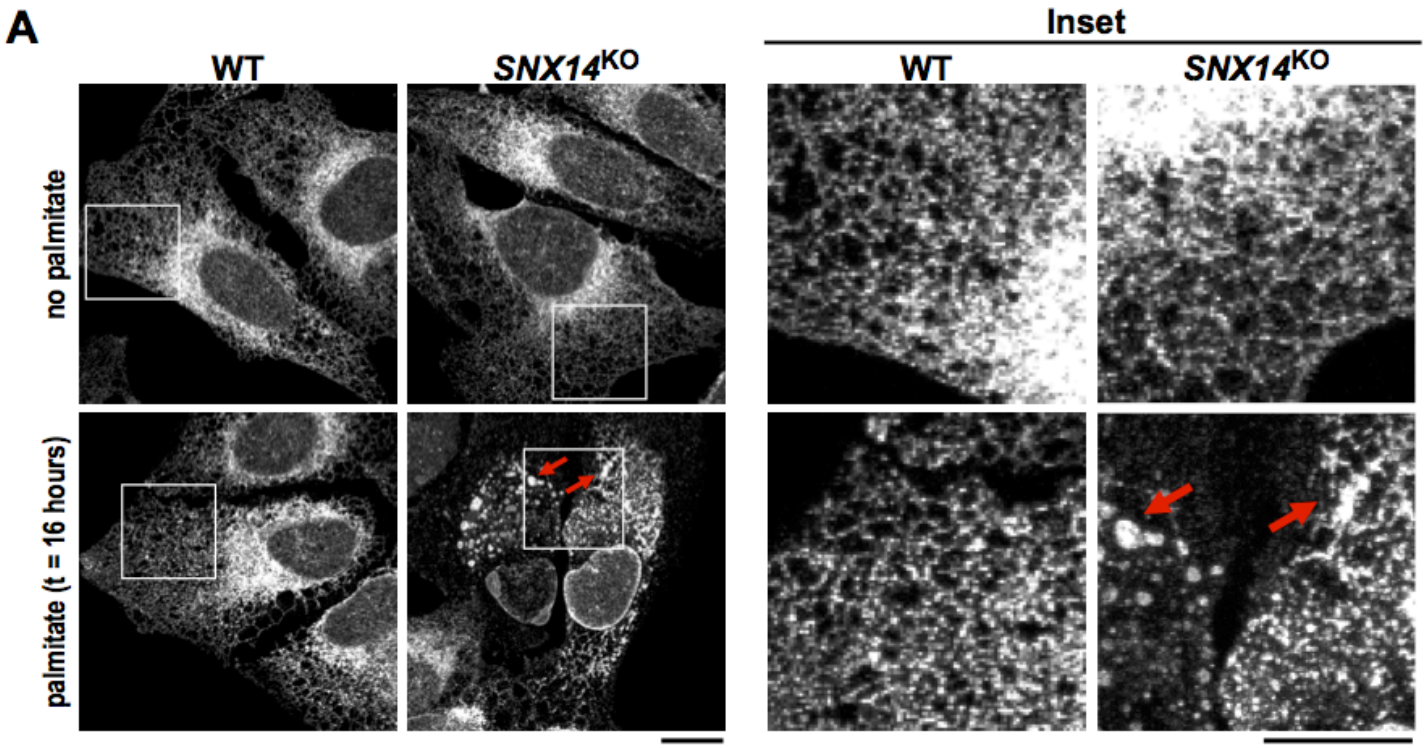

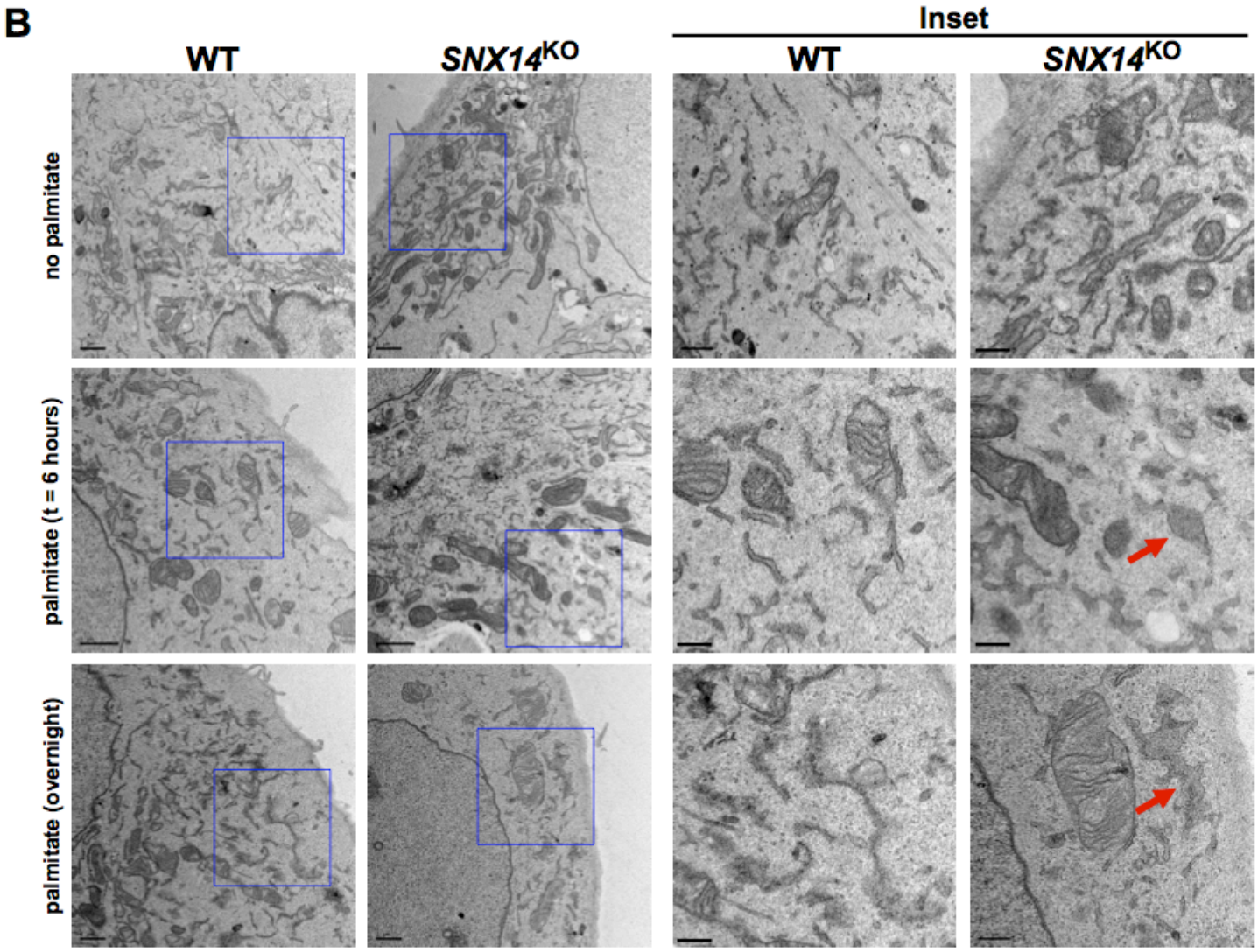

Figure 2

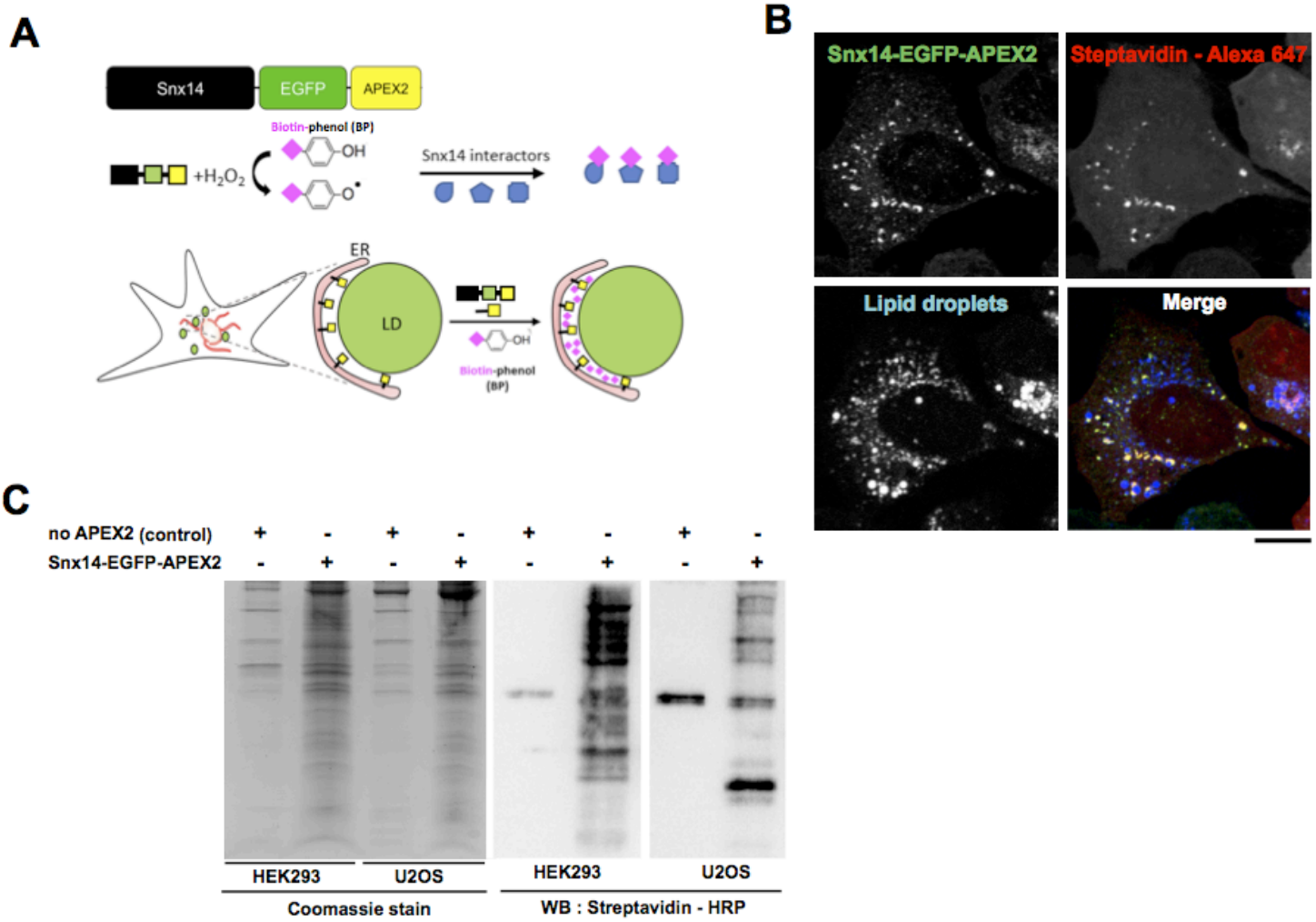

Figure 3

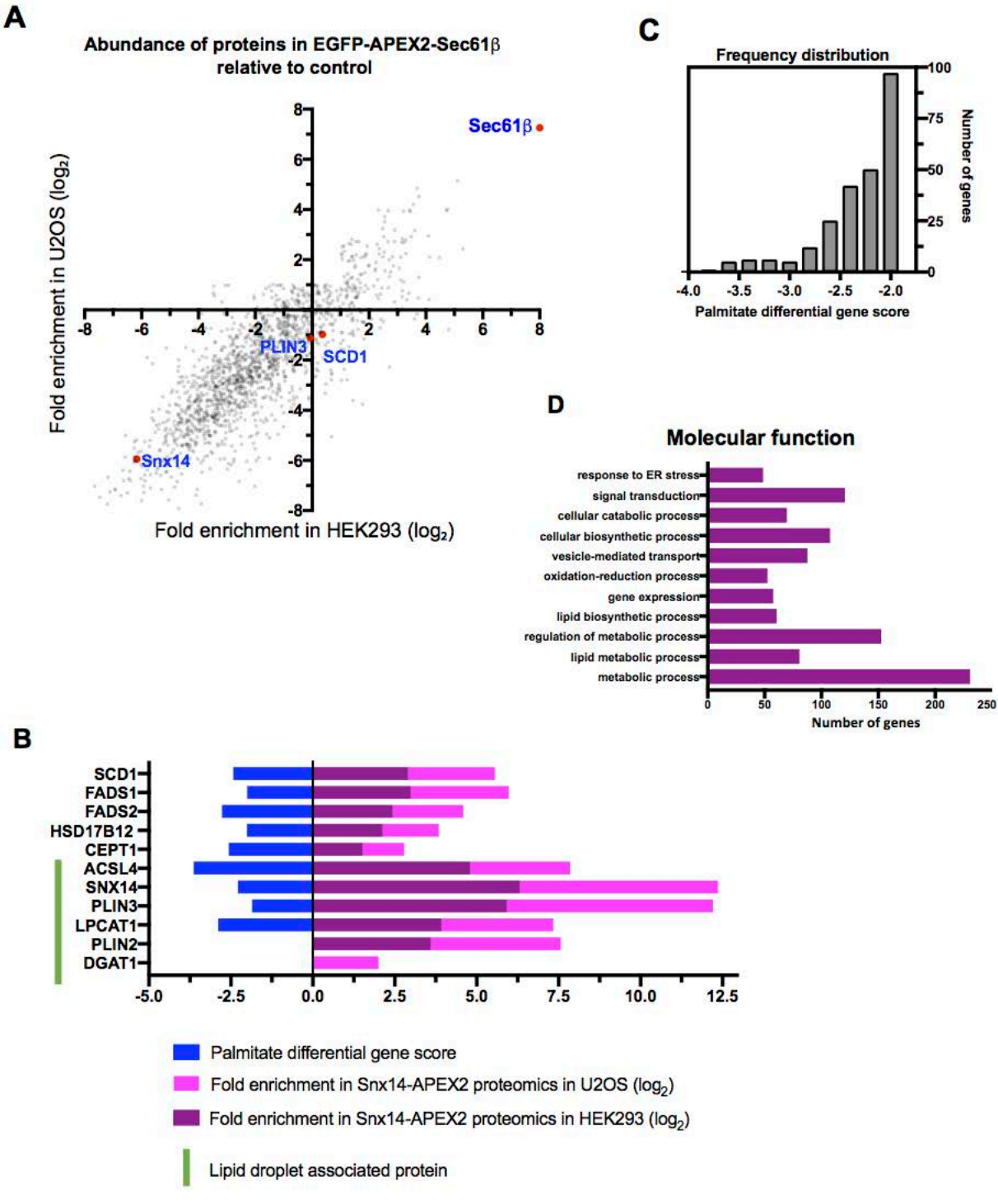

Supplementary Fig 3

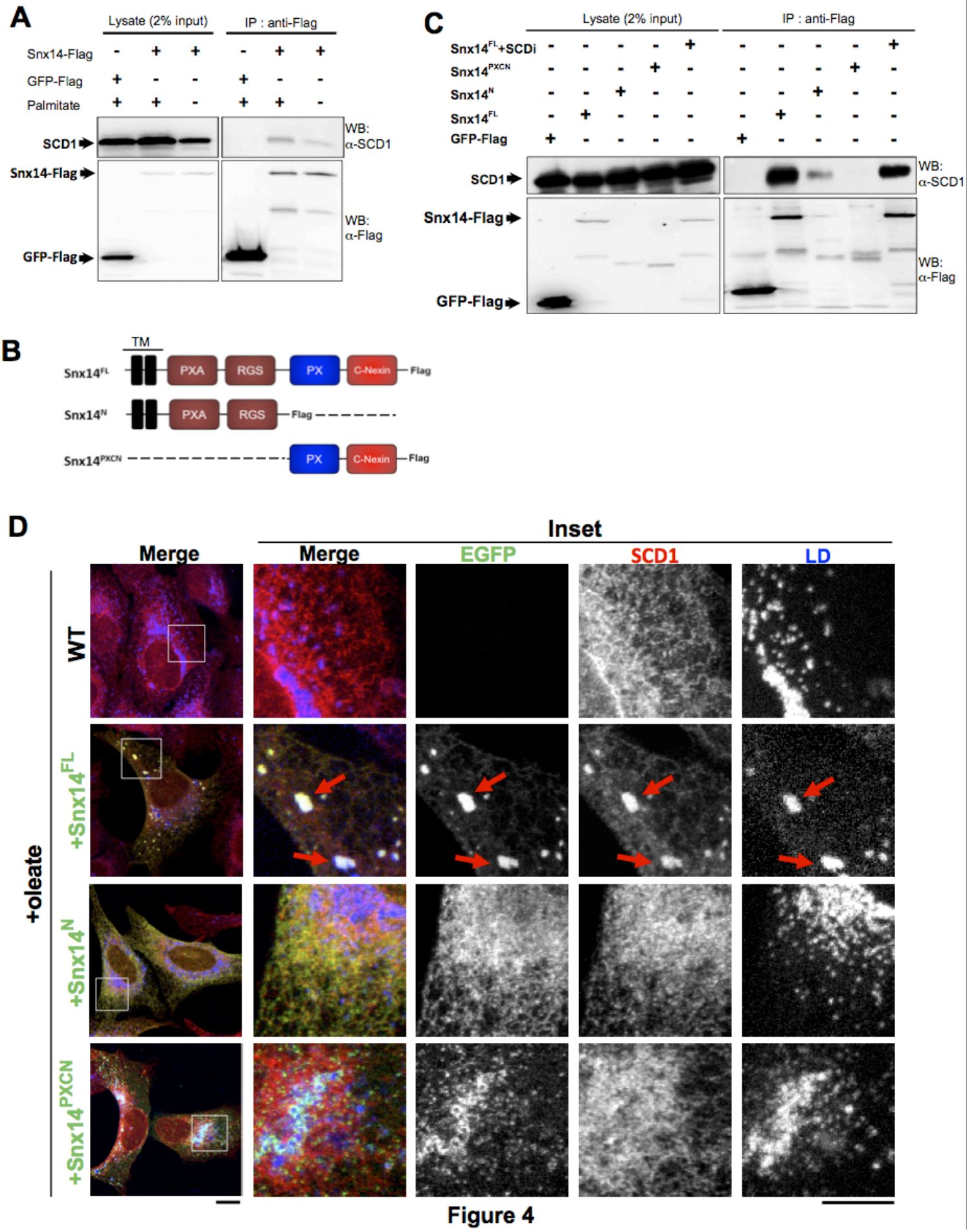

Figure 4

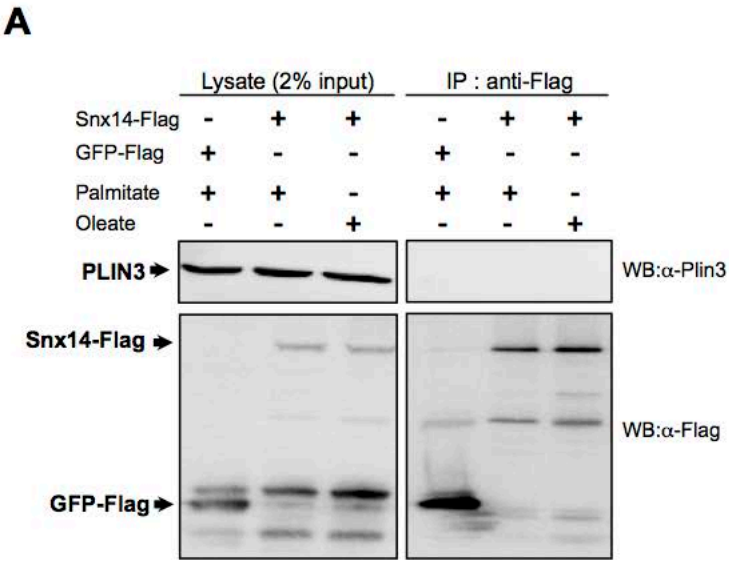

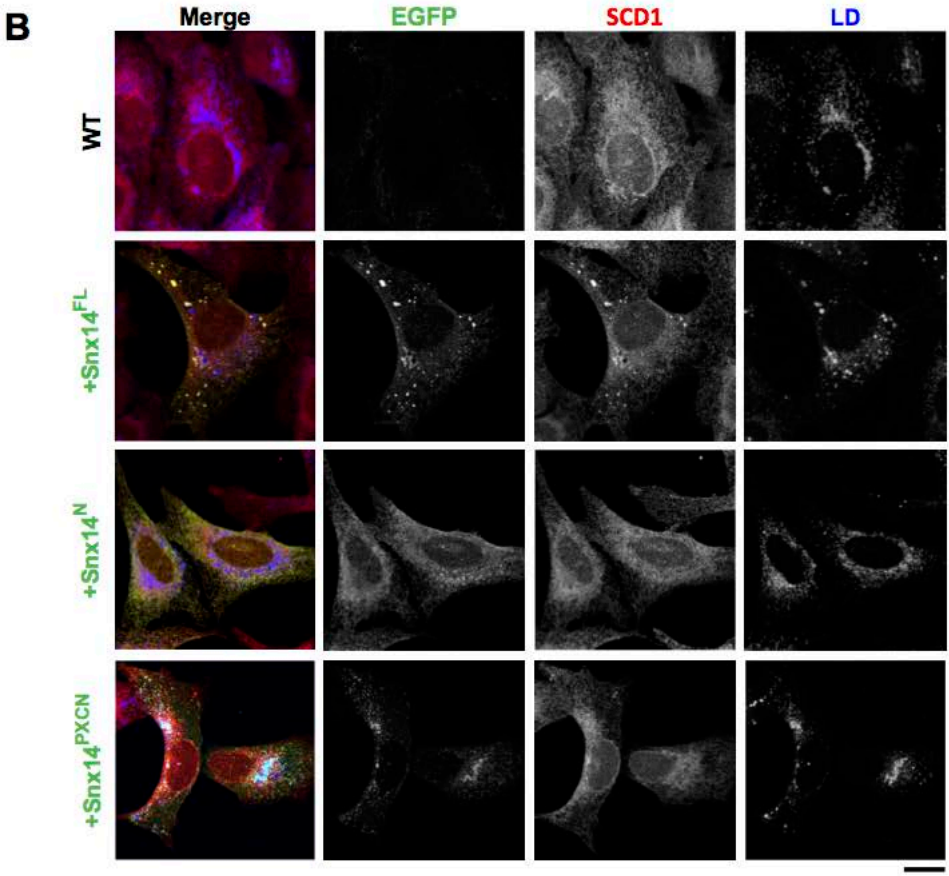

Supplementary Figure 4

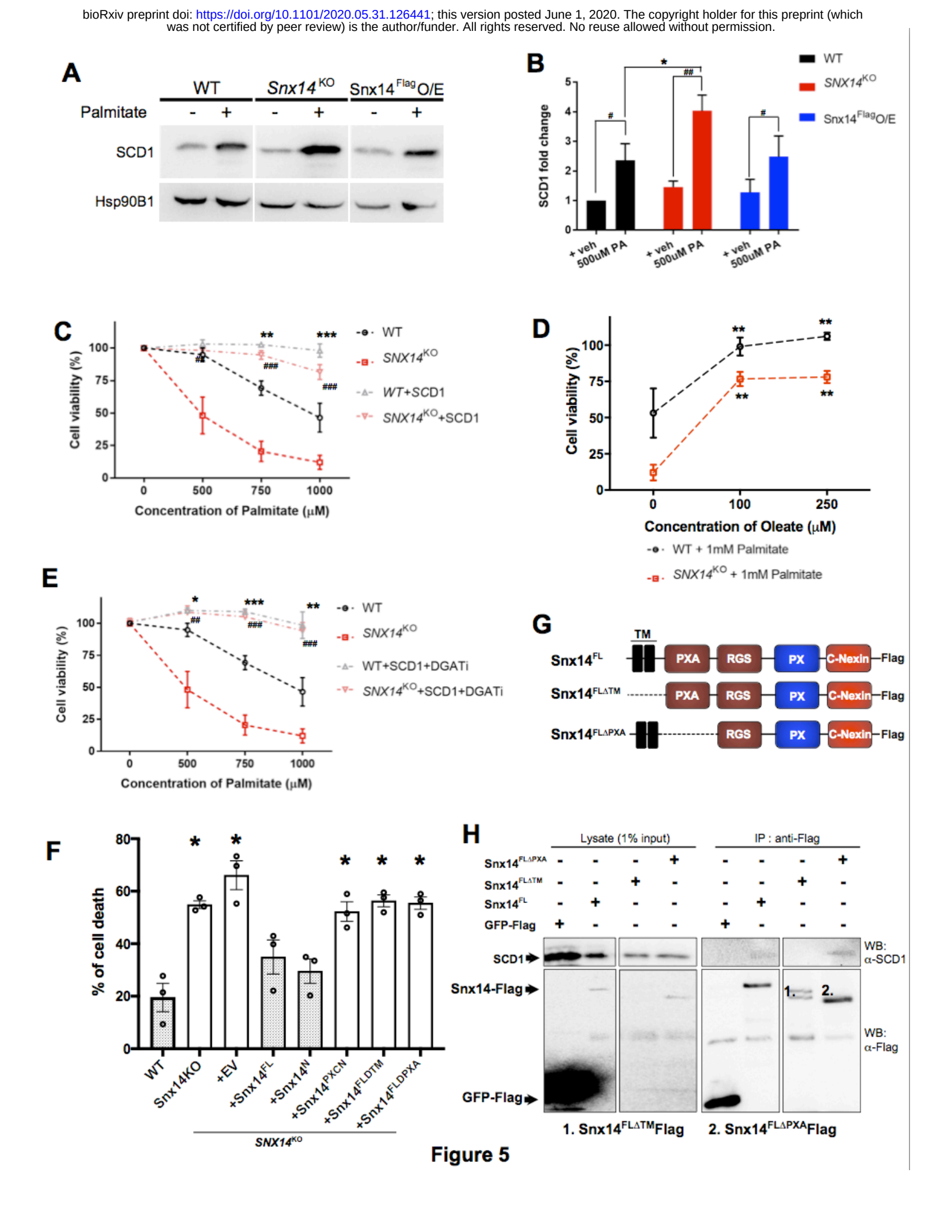

Figure 5

A

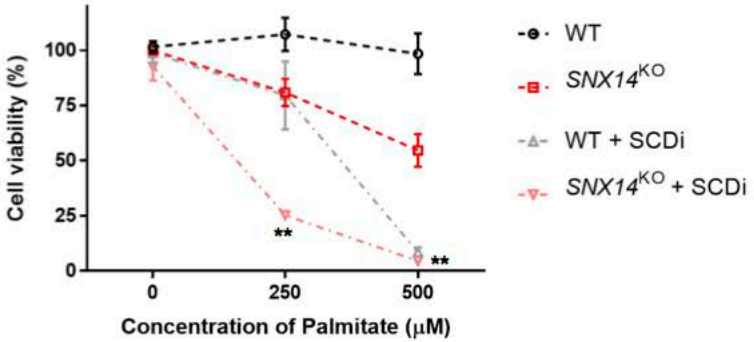

Supplementary Figure 5

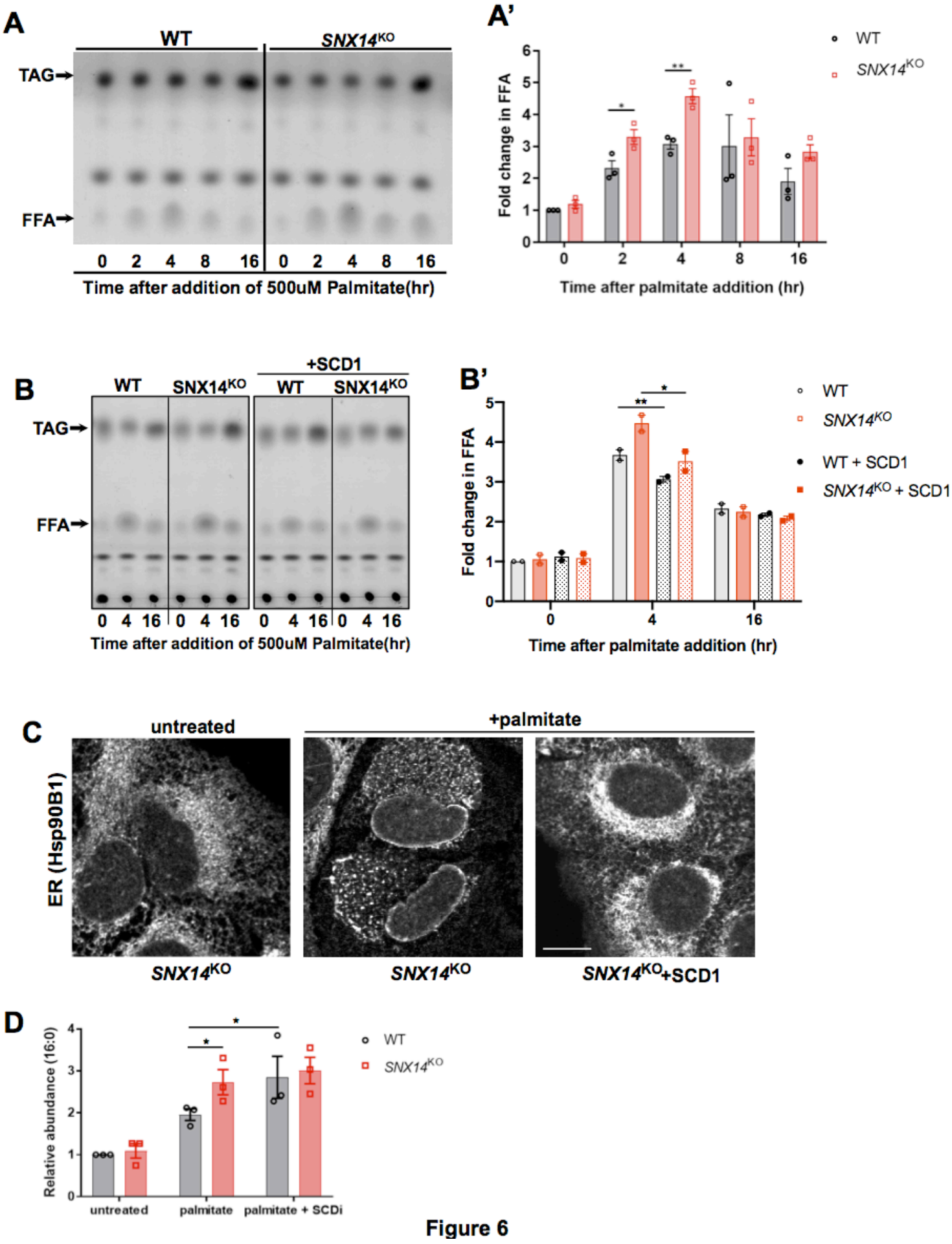

Figure 6

A

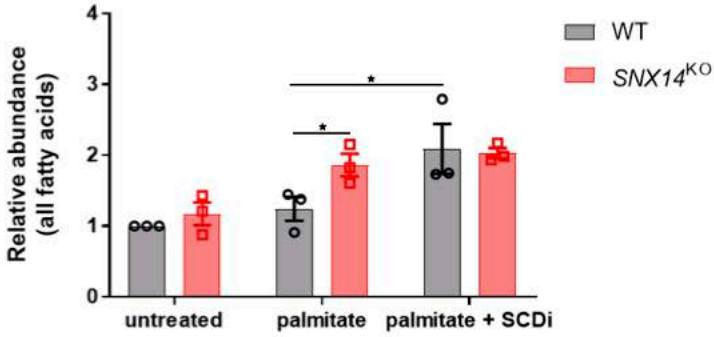

Supplementary Figure 6

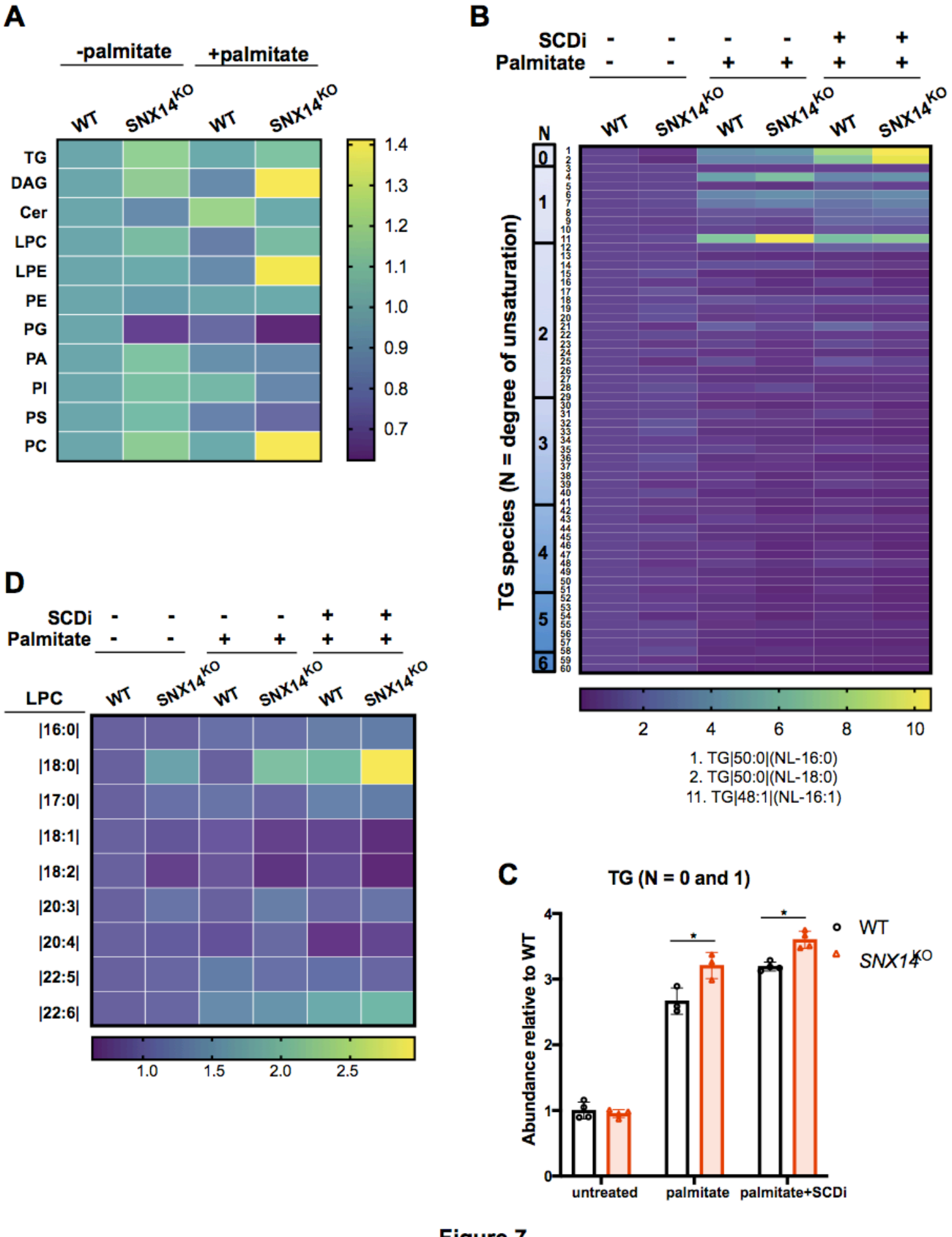

Figure 7

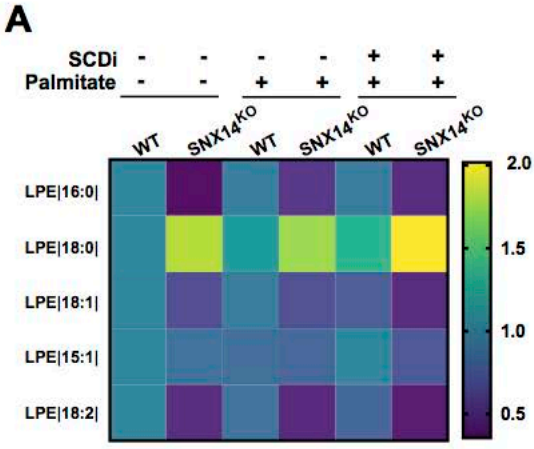

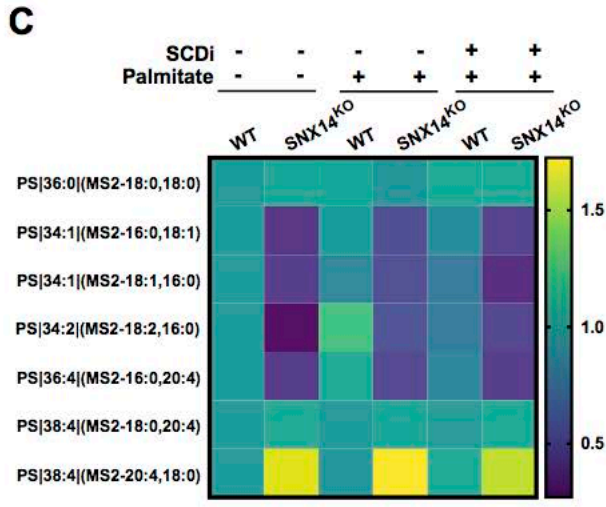

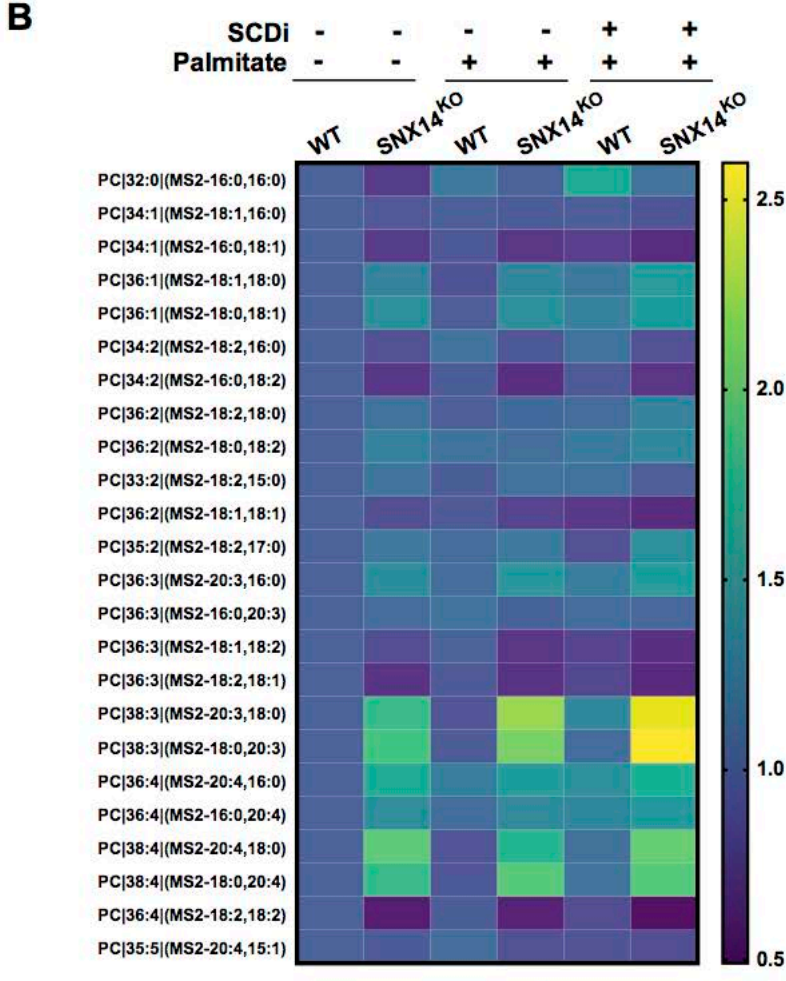

Supplementary Fig 7

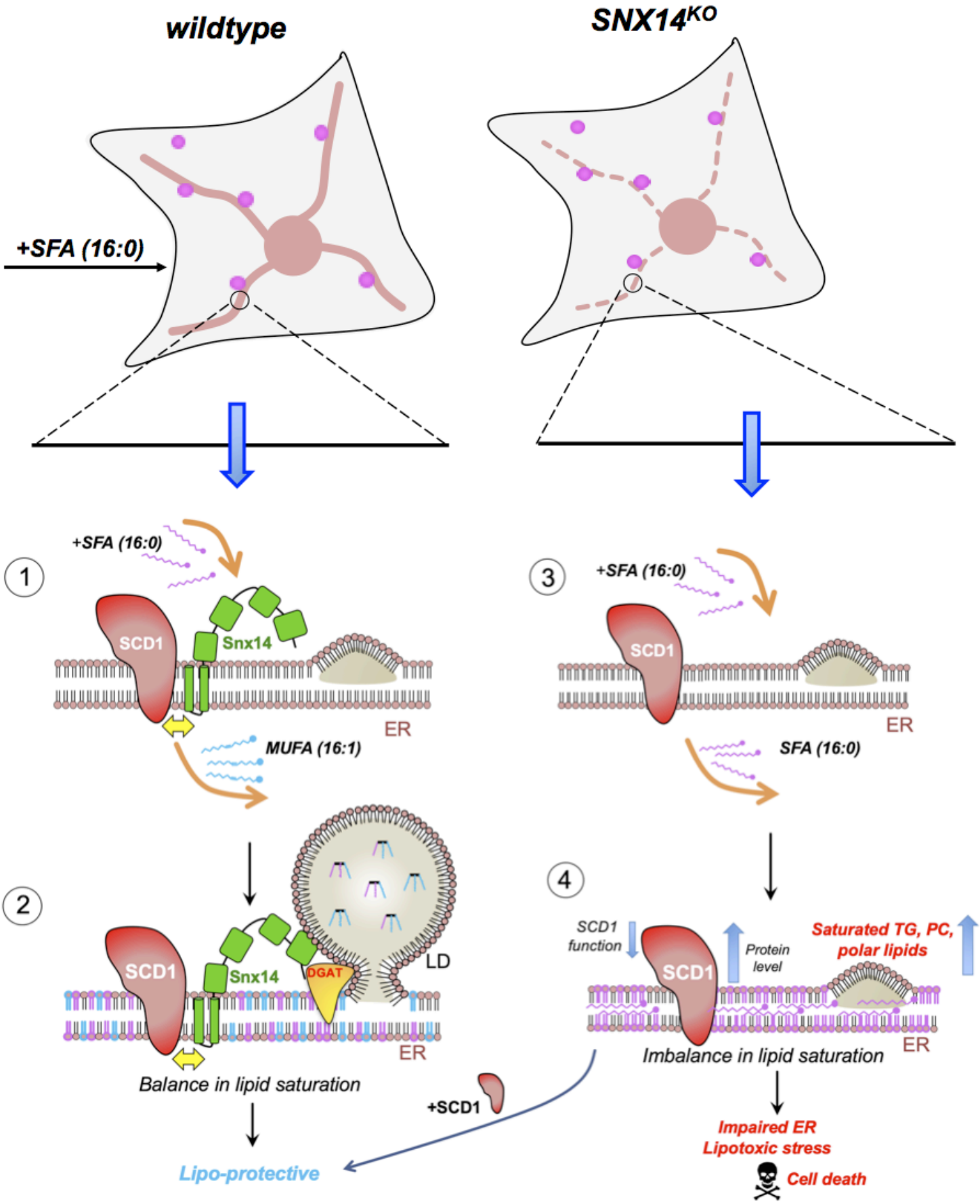

Figure 8